Journal of Environmental Chemical Engineering 11 (2023) 111308

Contents lists available at ScienceDirect

Journal of Environmental Chemical Engineering

journal homepage: www.elsevier.com/locate/jece

Synthesis of N-doped TiO_2 nanoparticles with enhanced photocatalytic activity for 2,4-dichlorophenol degradation and H_2 production

Javed Ali Khan [a,*], Murtaza Sayed [b], Noor S. Shah [c], Sanaullah Khan [d], Ashfaq Ahmad Khan [e], Muhammad Sultan [f], Ammar M. Tighezza [g], Jibran Iqbal [h], Grzegorz Boczkaj [i,j,**]

[a] Department of Chemistry, Abdul Wali Khan University Mardan, Mardan 23200, Pakistan
[b] Radiation Chemistry Laboratory, National Centre of Excellence in Physical Chemistry, University of Peshawar, Peshawar 25120, Pakistan
[c] Department of Environmental Sciences, COMSATS University Islamabad, Vehari Campus, 61100, Pakistan
[d] Department of Chemistry, Women University, Swabi 23430, Pakistan
[e] Department of Chemistry, Women University of Azad Jammu and Kashmir, Bagh 12500 Pakistan
[f] Department of Chemistry, Federal Urdu University of Arts, Science and Technology, Karachi, Pakistan
[g] Department of Chemistry, College of Science, King Saud University, P.O. Box 2455, Riyadh 11451, Saudi Arabia
[h] College of Interdisciplinary Studies, Zayed University, Abu Dhabi 144534, United Arab Emirates
[i] Department of Sanitary Engineering, Faculty of Civil and Environmental Engineering, Gdansk University of Technology, G. Narutowicza St. 11/12, 80-233 Gdansk, Poland
[j] EkoTech Center, Gdansk University of Technology, G. Narutowicza St. 11/12, 80-233 Gdansk, Poland

ARTICLE INFO

Editor: Isabel Oller Alberola

Keywords:
Nitrogen doped TiO_2
Chlorinated organic compounds
Environmental sustainability
Water treatment
Solar H_2 production
Circular economy

ABSTRACT

Nitrogen-doped titanium dioxide (N-TiO_2) nanoparticles were prepared using a modified sol-gel method. The as-prepared nanoparticles were characterized by state-of-the-art techniques for their optical, structural and morphological properties. The crystallite size, surface area and bandgap energy of reference TiO_2 and N-TiO_2 nanoparticles were found to be 16.1 and 10.9 nm, 83.6 and 131.8 $m^2\ g^{-1}$ and 3.23 and 2.89 eV, respectively. The photocatalytic activities, in terms of 2,4-dichlorophenol (2,4-DCP) degradation, of reference TiO_2 and N-TiO_2 were found to be 46.9% and 65.4% at 120 min of treatments under UV light irradiation and 21.5% and 77.6% at 240 min of treatment under visible light irradiation, employing 153.4 μM 2,4-DCP, 1 g/L photocatalyst dosage, and pH 5.6. Interestingly, considerable H_2 production rate (i.e., 386 μmol $h^{-1}\ g^{-1}$) was observed for visible/N-TiO_2 system in presence of 0.2 wt% Pt. The study revealed that visible/N-TiO_2 photocatalytic system can be used as an economically viable technology for environmental sustainability.

1. Introduction

Titanium dioxide (TiO_2) has been extensively studied as a nontoxic, inexpensive and highly effective photocatalyst for wastewater treatments [1,2]. However, TiO_2 can utilize only 4–5% of the total sun light (i.e., only ultra violet (UV) fraction) because of its wide bandgap energy (3.2 eV for anatase form) [3,4]. Moreover, the rate of recombination of photo-generated electron-hole (e^-/h^+) pair is very large for pure TiO_2 [5].

Therefore, it is highly desirable, but highly challenging too, to develop visible light active photocatalysts. In the last few decades, researchers have explored new methods of extending the photo-response of TiO_2 from UV to visible light region (≈ 45% of the total solar spectrum) [4,6]. The most frequent method used for this purpose is doping TiO_2 with metals (Co, Cr, Cu, Mo, Fe, Mn, Zn, W, V etc.) [7–12] and nonmetals (C, N, F, P, S etc.) [4,5,13–16]. Doping with foreign elements can tune the optoelectronic properties of TiO_2 which in turn boosts its photocatalytic efficacy under visible light illumination [1,4]. Since costly ion-implantation resources are needed for the synthesis of transition metal-doped TiO_2, more efforts had been paid to non-metal doping TiO_2 [1,4]. Doping TiO_2 with non-metals has been deemed as an effective strategy for the synthesis of visible light active TiO_2 nanoparticles [17,18]. Among non-metals, N, B, C, S, F, I and Cl, due to their large electronegativity, have been proved to be promising doping candidates for increasing the photocatalytic activity of TiO_2 under visible

* Corresponding author.
** Corresponding author at: Department of Sanitary Engineering, Faculty of Civil and Environmental Engineering, Gdansk University of Technology, G. Narutowicza St. 11/12, 80-233 Gdansk, Poland.
E-mail addresses: javedkhan@awkum.edu.pk, khanjaved2381@gmail.com (J.A. Khan), grzegorz.boczkaj@pg.edu.pl (G. Boczkaj).

https://doi.org/10.1016/j.jece.2023.111308
Received 17 June 2023; Received in revised form 5 September 2023; Accepted 21 October 2023
Available online 26 October 2023

light illumination [19]. This enhancement has been ascribed to: (i) decrease in the rate of e^-/h^+ pair recombination; (ii) shifting the bandgap energy towards visible light region by bringing the valence band (VB) of TiO_2 upwards; (iii) introducing new mid-gap states which serve as electron donors or electron acceptors in the TiO_2 bandgap; and (iv) widening the absorption capacity of TiO_2 towards the visible light portion [19,20]. In short, non-metal doping is generally used to improve the optoelectronic properties of TiO_2 to increase its photocatalytic activity under visible light irradiation.

Being equivalent in atomic size with oxygen atom and having low ionization energy, nitrogen atom is considered to be a promising doping candidate to alter the optical properties of TiO_2 and diminish the electron-hole pairs recombination rate [21–23]. It has been found that N doping can induce localized energy states in the bandgap (i.e., between the valence and conduction bands) of TiO_2 [24]. These localized energy sates enhance the photocatalytic efficiency of nitrogen doped TiO_2 (N-TiO_2) under visible light via reducing the energy needed for the excitation of electrons. Nitrogen atoms can be present as neutral paramagnetic ($N^\bullet$) or negatively charged diamagnetic (N^-) centers in N-TiO_2 lattice. Both of these centers contribute to the improvement of photocatalytic activity of N-TiO_2 under visible light illumination by inducing the localized energy states in the bandgap of N-TiO_2 thereby shifting the bandgap energy from UV region to visible light region. Moreover, both substitutional and interstitial positions can possibly be occupied by nitrogen atoms in the TiO_2 crystal lattice [24; 25]. It has been found that interstitial sites are generally preferred over substitutional ones under the condition of excess nitrogen and oxygen [24,26]. However, substitutional sites are possibly preferred over interstitial sites under extreme reducing conditions, e.g., annealing at high temperature [26].

In accordance of the density functional theory (DFT) calculations, carried out by Di Valentin et al. [24], the substitutional N-atom is attached to three titanium (Ti) atoms in the lattice (also expressed as Ti−N − Ti or or N − Ti−O linkages) [27] and therefore, replaces an O-atom of TiO_2. The bond lengths of Ti−N were calculated to be a bit lengthier than that of Ti−O (i.e., 1.964 and 2.081 Å for Ti−N compared to 1.942 and 2.002 Å for Ti−O). The substitutional nitrogen atom has been considered to be in negative oxidation state (N^{3-}) [25,28]. On the other hand, N atom is attached to one O and two Ti atoms in the interstitial model (expressed as O−Ti−O−N or Ti−O−N or N − O linkages) [27,29–32]. The N-O bond was found to be 1.36 Å. The interstitial nitrogen atom existed in positive oxidation state. Furthermore, the energies of localized energy states created by the doped N-atoms depends on the nature of N-atoms. The localized energy states of the substitutional N-atoms are at 0.14 eV above the top of the VB of TiO_2, whereas those of the interstitial N-atoms are at 0.73 eV above the top of the VB of TiO_2. It has been found that electronic excitations are possible from the localized energy states of nitrogen to the conduction band (CB) of TiO_2. Similarly, there can be electronic excitations from the VB of TiO_2 to the localized impurity states of nitrogen [25,26]. This is because, the localized impurity states of nitrogen are partially vacant. The electronic excitations from localized nitrogen-impurity states to the TiO_2 CBs lead to the formation of e^-/h^+ pairs, thereby contribute to the photocatalytic efficiency of N-TiO_2. Whereas, the electronic excitations from VB of TiO_2 to the localized nitrogen-impurity states do not lead to the photocatalytic reactions but rather reduces the utilization efficiency of light because the excited electrons fall back quickly to the VB of TiO_2 [25]. However, it has been assumed that electronic excitation from VB of TiO_2 to the nitrogen-impurity states could possibly contribute to the photocatalytic process via tandem effect if high energy photons are supplemented with low energy radiations [25]. In this tandem process, the low energy radiations would excite electrons from the VBs of TiO_2 to the nitrogen-impurity states whereas high energy radiations would further excite these electrons from the impurity states of nitrogen to the CB of TiO_2.

Huang et al. [23] synthesized N-TiO_2 nanoparticles by hydrothermal method and then applied them for the removal of rhodamine B and tetracycline. N-TiO_2 was more active than reference TiO_2 and P-TiO_2 in degrading rhodamine B and tetracycline under UV and visible light irradiation. For rhodamine B, the calculated rate constants were 11.36×10^{-2} and 6.35×10^{-2} min^{-1} under UV radiation for N-TiO_2 and reference TiO_2, respectively. Similarly, the degradation rate constants of rhodamine B were found to be 1.99×10^{-2}, 0.63×10^{-2} and 0.58×10^{-2} min^{-1} for N-TiO_2, reference TiO_2 and P25 (commercial TiO_2), respectively, under visible light irradiation. For tetracycline, the degradation rate constants were calculated as 8.96×10^{-2}, 1.18×10^{-2} and 2.75×10^{-2} min^{-1} for N-TiO_2, reference TiO_2 and P25 under visible light illumination, respectively. Bakre et al. [21] observed that N-TiO_2 was more active than P25 in removal of methylene blue with calculated rate constants as 0.0342 and 0.0206 min^{-1} for N-TiO_2 and P25, respectively. Other researchers have also found higher reactivity for N-TiO_2 than reference TiO_2 and/or P25 [1,33–37].

The aim of this study was to prepare visible light responsive N-doped TiO_2 (N-TiO_2) nanoparticles by a modified sol-gel method. The as-prepared N-TiO_2 samples were characterized by state-of-the-art instruments for structural, morphological, and optoelectronic properties. The N-TiO_2 photocatalyst was then applied for the degradation/removal of 2,4-dichlorphenol (2,4-DCP). Since chlorophenols are considered to be toxic organic compounds and have been listed as priority water contaminants by the United States Environmental Protection Agency (USEPA), 2,4-DCP was selected as a model contaminant for the present study [38]. The photocatalytic efficiency of N-TiO_2 was compared with reference TiO_2 (synthesized under similar experimental conditions except using the source of nitrogen). The study investigates the kinetics and mechanism of 2,4-DCP degradation in detail. The relative contribution of each reactive species towards 2,4-DCP degradation was calculated. The plausible degradation mechanism was proposed on the basis of degradation products of 2,4-DCP detected here. The toxicity of 2,4-DCP treated solutions was ascertained by studying the bioluminescence inhibition of *Vibrio fischeri* (a marine photobacterium). In addition, Ecological Structure Activity Relationship (ECOSAR) program was used to assess the toxicological behavior of 2,4-DCP and its detected products (DPs) towards aquatic organisms. N-TiO_2 photocatalyst was also assessed for solar hydrogen production.

2. Experimental

2.1. Reagents

Commercial TiO_2 (Degussa-P25) powder, titanium tetraisopropoxide (TTIP) (97%) and polyoxyethylene (80) sorbitan monooleate (a nonionic surfactant, commonly known as Tween 80) were received from Sigma Aldrich, USA. Triethylamine (TEA) and acetic acid (AA) were purchased from Fisher Scientific, iso-propanol (i-PrOH, 99.8%) from Pharmco, 2,4–dichlorophenol, benzoquinone, triethanolamine and methanol from Merck, and 2–chlorophenol, 4–chlorophenol, phenol, catechol and hydroquinone from Fluka. In this work, analytical grade reagents and chemicals were used. Standard and working solutions were prepared in Milli-Q water (resistivity = 18.2 MΩ cm, Millipore system, USA).

2.2. Preparation of nitrogen-doped TiO_2 nanoparticles

A modified sol-gel method was used for the synthesis of reference- and nitrogen-doped TiO_2 (N-TiO_2) nanoparticles. Titanium tetraisopropoxide (TTIP) and triethylamine (TEA) were used as Ti and N sources, respectively. Initially, Tween 80- a pore directing agent- was taken in a beaker followed by the dropwise addition of iso-propanol (i-PrOH) while mixing the solution vigorously using a magnetic stirrer. The solution was stirred vigorously until the complete dissolution of Tween 80. Following the dropwise addition of i-PrOH, acetic acid (AA) was poured into solution instantly to sustain a low pH (~ 6.4). The addition of AA to i-PrOH solution also results in "in situ" production of water molecules

via esterification reaction between i-PrOH and AA. Then, TEA was introduced dropwise into the reaction solution. The subsequent solution was mixed vigorously for 1 h. Finally, TTIP was added into the above solution while stirring it vigorously. The resulting solution was stirred for 24 h at ambient temperature to obtain a stable, transparent and homogenous solution. Subsequently, the final stable solution was dried at 22 ± 1 °C for 24 h. The dried sol was then calcined in a furnace, having multi-segment programmable option (Paragon HT-22-D, Thermcraft). Initially, the temperature was raised at a ramp rate of 50 °C/h from room temperature to 100 °C and upheld at 100 °C for 1 h. Then, the temperature was elevated from 100 to 400 °C at a ramp rate of 60 °C/h, hold for 2 h at 400 °C and finally cooled down in a natural manner to get a yellowish N-TiO_2 samples. The chemicals were taken in molar ratio of TTIP:Tween 80:i-PrOH:AcOH:TEA = 10:3.6:135:25:20. The same method and same molar ratio of the chemicals was applied while preparing the reference TiO_2 without adding TEA. It has been reported that catalysts could maintain their anatase phase at the highest temperature used in this method for the preparation of N-TiO_2 [39]. All organic compounds were expected to be removed from the reference TiO_2 and N-TiO_2 during calcination. The calcined reference TiO_2 and N-TiO_2 nanomaterials were scraped from the glass dishes and grinded into fine powders.

2.3. Characterization of the as-synthesized nanoparticles

X-ray diffraction (XRD, X′Pert PRO; Philips) with Cu K (λ = 1.54 Å) radiation was used for finding out the structural properties of the reference TiO_2 and N-TiO_2 nanoparticles. BET (Brunauer-Emmett-Teller) surface area, BJH (Barrett-Joyner-Halenda) pore size, porosity, pore volume, and pore size distribution were determined by a porosimeter analyzer (Tristar 3000, Micromeritics). Prior to the analysis of the samples (synthesized nanoparticles) by porosimeter analyzer, the sample powders were purged with N_2 gas via Flow prep 060 (Micromeritics) at 150 °C for 2 h.

The optical properties and bandgap energies of reference TiO_2 and N-TiO_2 samples were determined by UV–vis spectrophotometer (2501 PC, Shimadzu). Barium sulfate ($BaSO_4$) was used as a reference material in the UV–visible spectra analysis.

The information about crystal structure and crystal size of the nanomaterials was acquired from the HR-TEM (A JEM-2010 F (Jeol)) results. The field emission gun of HR-TEM was operated at 200 kV. For samples preparation, the nanomaterials were dispersed in HPLC grade methanol by ultrasonication (2510R-DH; Bransonic) for 30 min. An infrared lamp was then used to dry the sample solution, fixed on carbon-coated copper grid (LC325-Cu, EMS). The chemical composition and valence state of the dopant in the TiO_2 powder were revealed by analyzing the samples by XPS (SSX-100 XPS). In XPS analysis, monochromatic radiations of Al Kα having 1486.6 eV energy and X-rays having beam diameter = 600 μm were used. The C 1 s level peak at 284.6 eV was used for calibration of absolute binding energies. FTIR spectrometer (FTIR-8400S, Schimadzue) was used for investigating the occurrence of nitrogen in the N-TiO_2 samples.

2.4. Determination of photocatalytic activity

To assess the photocatalytic efficiency of the synthesized N-TiO_2 samples, photocatalytic degradation of 2,4-DCP was studied under UV and visible light irradiations. Two low-pressure mercury UV lamps (Spectronics), 15 W each one, were used as UV irradiation sources, emitted light at 365 nm. The radiation intensity of the UV lamps was determined with the help of a radiant power meter (Newport Corporation) and was calculated as 2.6×10^{-4} W cm^{-2}. As visible light sources, two fluorescent lamps (Cole-Parmer), 15 W each one, were used to irradiate the reaction solution. A UV block filter (UV420, Opticology) was used to eliminate the entrance of UV radiation into the reaction solution. The visible light intensity was found to be 7.5×10^{-4} W cm^{-2}, calculated with radiant power meter (Newport Corporation). The reactor was a Pyrex® glass beaker containing 50 mL of the reaction solution. The 2,4-DCP concentration was 153.4 μM (25 mg/L), the photocatalyst loading was 1 g/L, the pH was 5.6 (unadjusted) and H_2O_2 concentration (when used) was 2 mM. During the course of reaction, the working solution was properly mixed using a magnetic stirrer. 1 mL of irradiated samples were collected at pre-determined time intervals. 0.3 mL of methanol was added to the collected irradiated samples to avoid further reaction. 0.2 μm pore size syringeless filters (Whatman) were then used to filter out the catalyst particles from the collected irradiated samples. HPLC (Agilent Series 1100), equipped with diode array detector and a C18 column (150 mm × 3.9 mm), was used for quantification of 2,4-DCP in the irradiated samples. A mixture of methanol and 5% aqueous solution of acetic acid (v/v) (60:40, v/v) was used as mobile phase. The flow rate of the mobile phase was 1 mL/min. The wavelength of the detector was set at 280 nm.

Gas chromatography-mass spectrometry (Agilent Technologies 7890B-5977B) (GC-MS) was used for identification of the by-products of 2,4-DCP. The capillary column in GC-MS was HP-5MS (5% phenyl-methyl-siloxane). The dimensions of the column were: 30 m × 0.25 mm, 0.25 μm. Helium, used as a carrier gas, was set at a flow rate of 1.0 mL/min. The oven temperature was programmed as: 80 °C for 2 min, then increase to 180 °C @ 10 °C min^{-1} (3 min) and then rise to 280 °C @ 10 °C min^{-1} (5 min). Time for each run was 30 min. The temperature of the injector and ion source was fixed at 250 and 280 °C, respectively. Electron impact ionization was set at 70 eV and MS scan ranges from 50 to 550 *m/z*.

Ion chromatography (IC, Metrohm, Switzerland) was used for the determination of chloride ions (Cl^-) concentration in the treated samples. In IC, Cl^- were separated by Assup-5 column and detected by electrical conductivity detector. The details of the method can be seen in our previous publication [40].

Photocatalytic H_2 production experiments were performed at ambient pressure and temperature in a 500-mL Pyrex glass reactor. The Pyrex glass reactor was linked to gas chromatography (GC, Agilent 7890 A). 1 g L^{-1} N-TiO_2 was added to 100 mL aqueous solution of methanol. H_2PtCl_6 was directly dissolved in the above 100 mL reaction solution to achieve 0.2 wt% Pt solution, being used as a co-catalyst [41]. The volume ratio of methanol to total reaction solution was 1:5 (i.e., 20 mL methanol per 100 mL reaction solution). A visible light source (300 W Xe arc lamp) was used to initiate the photocatalytic H_2 production reaction. A UV cut-off filter (UV420, Opticology) was used to filter out photons of wavelength < 400 nm. The lamp was fitted at a distance of 20 cm from the Pyrex glass reactor. The intensity of the lamp was found to be 85 mW/cm^2. The solution was purged with N_2 gas for about 30 min before irradiation to attain anaerobic condition. The H_2 gas was detected by GC equipped with a thermal conductivity detector (TCD) and 5 Å molecular sieve column. The nitrogen was used as a carrier gas. The apparent quantum efficiency (AQE) of H_2 formation was determined under similar experimental conditions. However, instead of Xe arc lamp, three low-power UV-LED lamps (3 W each one, emitted light at 360 nm) (Shenzhen Warner JPLED Co. Ltd. China) were used as sources of UV-A light for AQE determination. Eqs. (1), (2a) and (2b) were used for calculation of AQE [42,43]:

$$n_{photons} = \frac{P\lambda}{hc} \times t \quad (1)$$

$$AQE(\%) = \frac{\text{number of reacted electrons}}{\text{number of incident photons}} \times 100 \quad (2a)$$

$$AQE(\%) = \frac{2(\text{number of evolved hydrogen molecules})}{\text{number of incident photons}} \times 100 \quad (2b)$$

where P, λ, c, h and t are the input power of light source, wavelength of light, speed of light, Planck's constant and irradiation time, respectively. 5.9 mW/cm^2 was found as intensity of each UV-LED lamp.

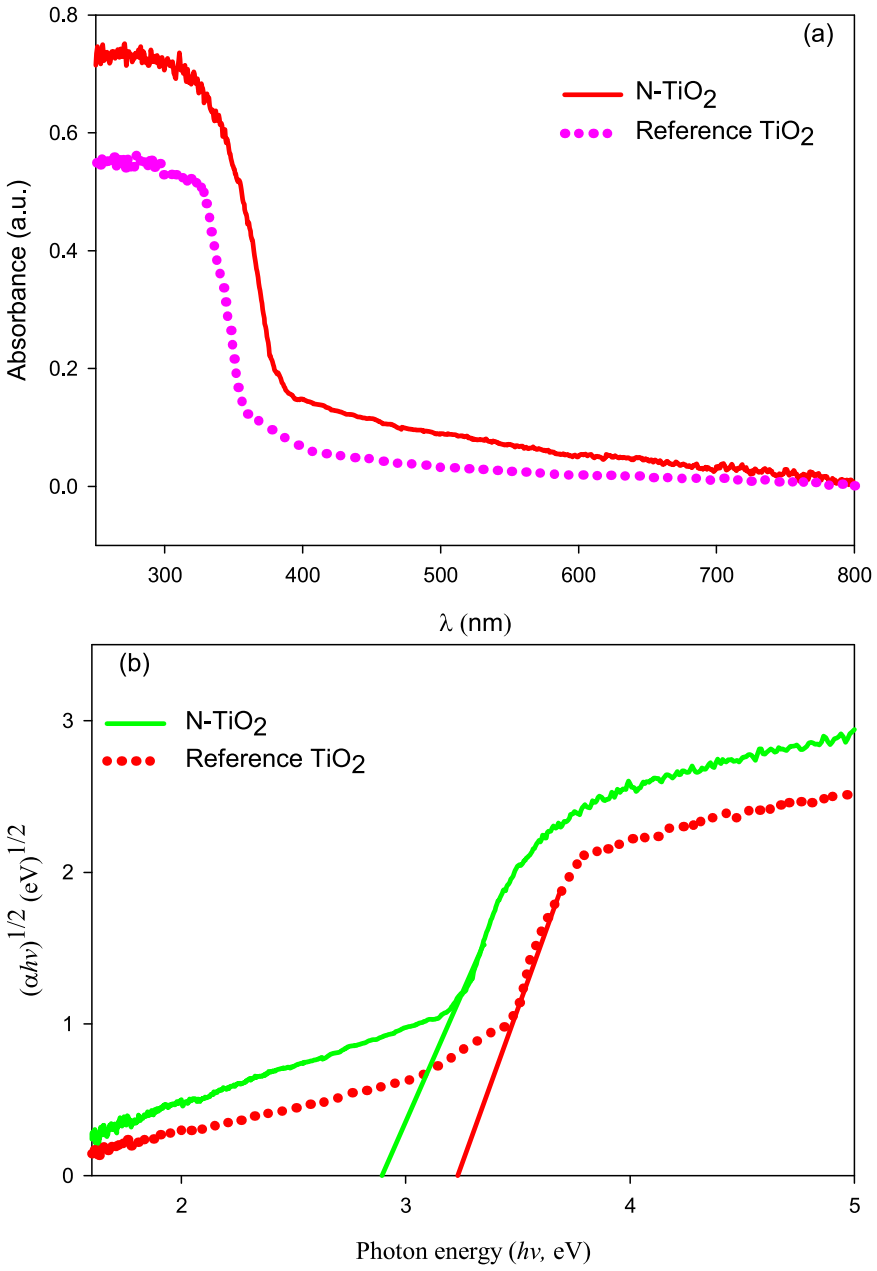

Fig. 1. (a) UV–vis absorption spectra of the N-TiO_2 and reference TiO_2 samples and (b) calculation of bandgap energy for indirect allowed transitions.

TOC analysis was performed with a Shimadzu TOC analyzer. To ensure the reproducibility of the results, each experiment was conducted three times.

2.5. Toxicity investigation

To evaluate the toxicity of the 2,4-DCP solutions treated by visible/N-TiO_2 process, a Microtox Toxicity Analyzer (Model 500, Azur Environmental) based on bioluminescence inhibition of *Vibrio fischeri* (a marine photobacterium) was used. The treated solution's pH was adjusted to 7 with NaOH solution. The treated samples were made saline with NaCl (2%, w/v). Prior to analysis, the samples (0.5 mL) were mixed with the bacterial suspension (0.5 mL), 50% (v/v) dilution of the irradiated samples. The samples were then incubated for 15 min at 15 °C. Finally, the reduction in the emission of light by the bacteria was measured. The results of the irradiated samples were compared with a non-toxic control solution (2% w/v NaCl). Finally, the percent relative inhibition (INH%) was calculated in accordance of the Karci et al. [44].

To get a deep insight into the toxicity of each individual detected byproduct of 2,4-DCP, the Ecological Structure Activity Relationship (ECOSAR) program was used [45]. This program successfully predicts the toxicities (both acute and chronic) towards three aquatic organisms namely fish, daphnia, and green algae. The acute toxicity is assessed in terms of contaminant concentration (in units of mg L^{-1}) responsible for the death of 50% daphnia and fish after 48 and 96 h exposure, respectively, represented by LC_{50}. Similarly, the acute toxicity towards green algae is estimated in terms of compound concentration (mg L^{-1}) responsible for the 50% growth inhibition of this microorganism after 96 h contact time, expressed as EC_{50} [46].

3. Results and Discussion

3.1. Morphological and structural properties of N-TiO_2 nanoparticles

The UV–vis absorption spectra of reference and nitrogen doped TiO_2 nanoparticles is presented in Fig. 1. It can be observed that nitrogen doping can increase the absorption of TiO_2 nano-powders in UV as well as visible light region, spectroscopically termed as blue shift and red shift, respectively. As a result, N-TiO_2 nanoparticles could be anticipated to possess higher visible light activity than reference TiO_2 nanoparticles. Furthermore, higher visible light absorption by N-TiO_2 could possibly indicate that nitrogen doping had lowered the bandgap of TiO_2. To verify this claim, the bandgap energies of both reference TiO_2 and N-TiO_2 were calculated by plotting $(\alpha h\nu)^{1/2}$ versus $h\nu$ (photon energy), considering indirect allowed transitions [47–49]. The high slopes of the plot curves were linearly extrapolated to determine the indirect bandgap energies. The bandgap energies were found to be 3.23 and 2.89 eV for reference TiO_2 and N-TiO_2, respectively. The lower bandgap energy of N-TiO_2 in comparison to reference TiO_2 is in agreement with the findings of the previous research studies [22,33,48–51]. Previously, the bandgap energy of N-TiO_2 nanoparticles was found to be 2.71 [22], 2.28 [48,50], 2.80 [49], 2.9 [51], and 2.83 eV [52]. From the calculated bandgap energies, we can conclude that the excitation wavelength of the TiO_2 nanoparticles changes from 384 nm (UV region, 3.23 eV photon energy) to 429 nm (visible region, 2.89 eV photon energy) via N-doping [18,50]. Thus, visible light photons could activate N-TiO_2 nanoparticles to generate electron-hole (e^-/h^+) pairs, capable of water contaminants degradation via a series of redox reactions. The lower bandgap energy of N-TiO_2 than reference TiO_2 is due to the additional localized energy states produced by the doped nitrogen atoms on the top of the VB of TiO_2, as mentioned earlier. If doped N-atoms occupy substitutional position, the N-impurity states will be located at 0.14 eV and at 0.73 eV if these doped nitrogen atoms occupy interstitial position in the crystal lattice of TiO_2. Thanks to these localized energy states produced by the

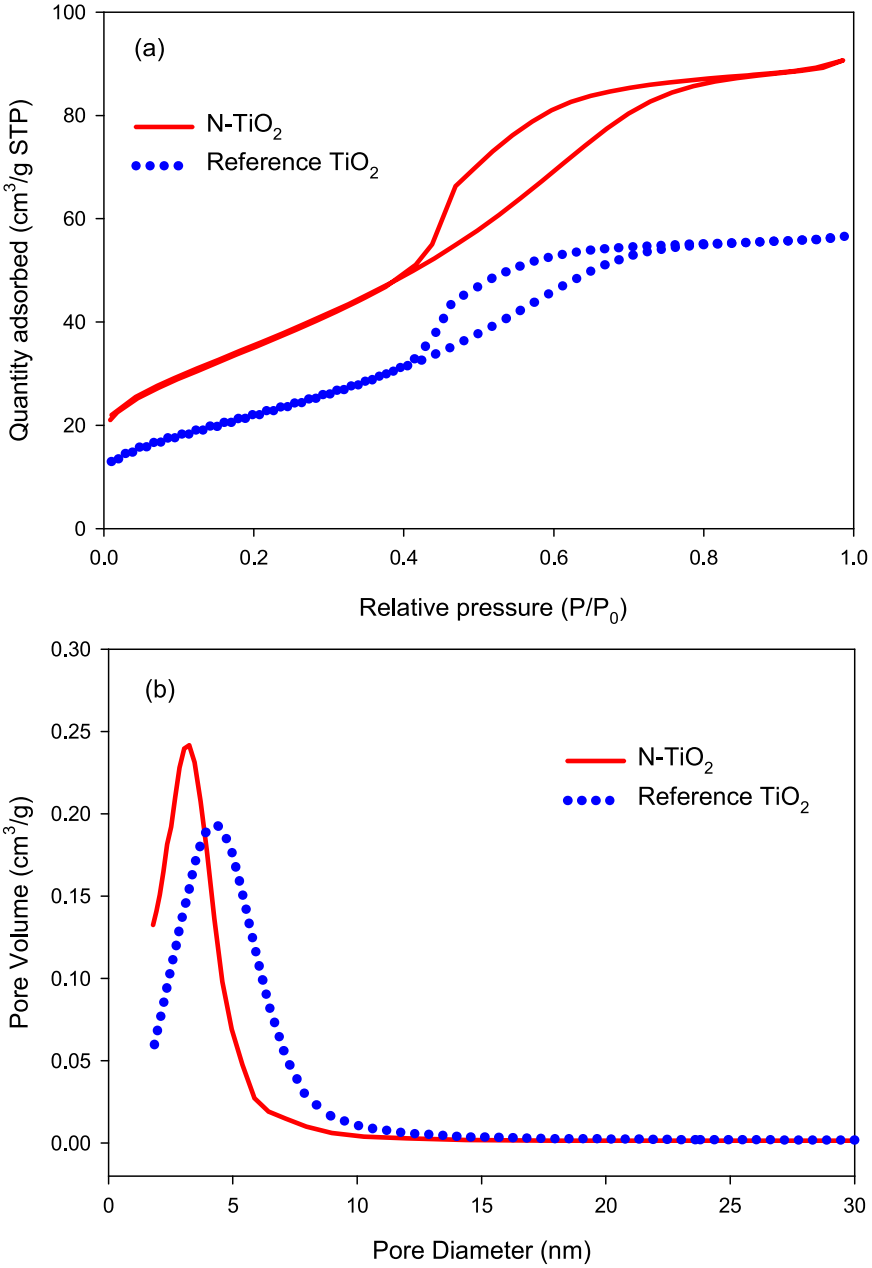

Fig. 2. (a) Nitrogen adsorption-desorption isotherms and (b) pore size distribution of as-prepared reference TiO_2 and N-TiO_2 nanoparticles.

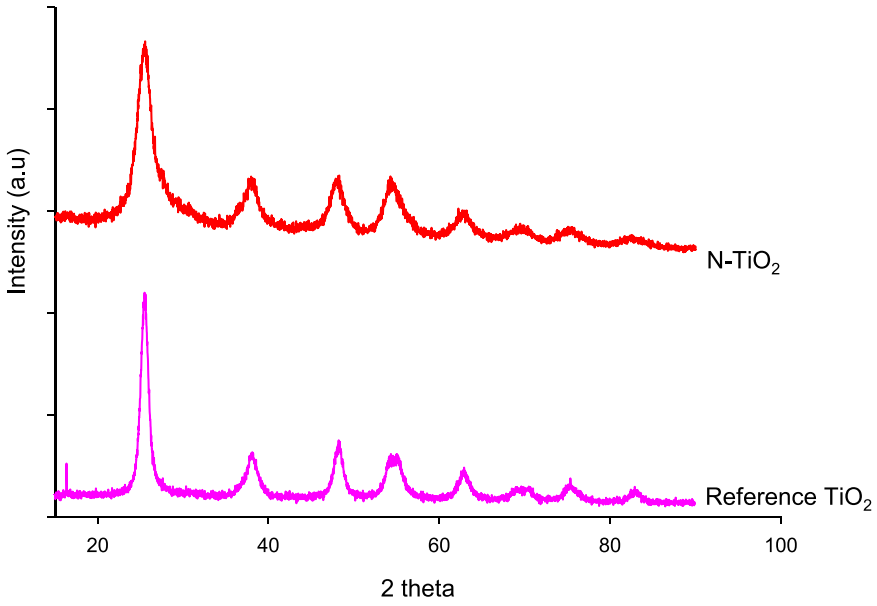

Fig. 3. XRD pattern of N-TiO_2 and reference TiO_2 nanoparticles.

doped nitrogen atoms which impart visible light activity to TiO_2 nanoparticles. Since solar spectrum comprises about 45% visible light, N-TiO_2 can use solar energy for photocatalytic degradation of environmental pollutants and for solar H_2 production. Thus, producing visible light active photocatalysts can bring down the cost of water treatments as well as of green water production.

The N_2 adsorption-desorption (AD) isotherms of the reference TiO_2 and N-TiO_2 nanoparticles is plotted in Fig. 2a. In accordance of IUPAC classification- on the basis of hysteresis loops- these N_2 AD isotherms are categorized as type IV [53]. Since type IV isotherm represents a mesoporous substance, the reference TiO_2 and N-TiO_2 samples are mesoporous in nature [53]. Applying the BJH method, the N_2 desorption isotherm was further used for calculation of pore size distributions using the Halsey equation. Fig. 2b shows that doping of the TiO_2 lattices with nitrogen atoms significantly changed the pore size distributions. Pore diameter of 4.3 and 3.2 nm were calculated for the reference TiO_2 and N-TiO_2 nanoparticles, respectively. The graph of pore size distribution, particularly for the N-TiO_2 nanoparticles, shows a narrow width which is an indication of good homogeneity of their pores.

Furthermore, the BET surface area analysis shows that N-doping significantly enhanced the BET surface area of TiO_2 nanoparticles from 83.6 m^2/g (reference TiO_2) to 131.8 m^2/g (N-TiO_2). Similarly, N-TiO_2 nanoparticles possess higher pore volume as compared to reference TiO_2 nanoparticles, i.e., 0.140 and 0.088 cm^3/g for N-TiO_2 and reference TiO_2, respectively.

Eq. (3) was used to calculate the average particle size of the synthesized reference TiO_2 and N-TiO_2 nanoparticles [49]:

$$D = \frac{6000}{\rho \times BET\ surface\ area} \tag{3}$$

where D is the average particle size and ρ is the density of the nanomaterial. For anatase form of TiO_2, the density has been reported to be 3.79 g cm^{-3} [54]. Using Eq. (3), the average particle sizes for N-TiO_2 and reference TiO_2 were found to be 12.0 and 18.9 nm, respectively.

Fig. 3 reveals the X-ray diffraction patterns of both N-TiO_2 and reference TiO_2 nanoparticles. Based on the diffraction peak at $2\theta = 25.5°$, a characteristic peak of (101) anatase crystal plane, it could be concluded that both reference TiO_2 and N-TiO_2 exhibited well-crystallized anatase structures. The XRD patterns did not show any peaks that could represent the rutile form of TiO_2. The XRD results suggested that the main TiO_2 phase was not affected by nitrogen doping. Moreover, the spaces of (101) plane (i.e., D (101)) for reference TiO_2 and N-TiO_2 were determined to be 3.53 and 3.52 Å, respectively (Table 1). Thus, the incorporation of nitrogen atoms into TiO_2 lattice did not significantly affect the dimensions of the unit cells of the TiO_2 lattices. This could possibly be owing to the low doping levels of nitrogen atoms in the TiO_2 lattice. The average crystallite size of N-TiO_2 and reference TiO_2 samples were calculated from the (101) plane of these samples using Scherrer formula, shown in Eq. (4)) [55]:

$$D = \frac{K\lambda}{\beta \cos\theta} \tag{4}$$

where D, K, λ, β and θ are the average crystallite size, a constant- equal to 0.89, wavelength of the X-ray radiation (1.54 Å), full width at half-maximum (FWHM) of 101 peak and diffraction angle, respectively

Table 1
Structural characteristics of N-TiO_2 and reference TiO_2 nanoparticles.

Catalyst type	Crystal phase	S_{BET} ($m^2\ g^{-1}$)	Crystal size (nm)[a]	Particle size (nm)[b]	Total pore volume ($cm^3\ g^{-1}$)	Porosity (%)[c]	D (101) (Å)[d]
N-TiO_2	Anatase	131.8	10.9	12.0	0.140	34.7	3.52
Reference TiO_2	Anatase	83.6	16.1	18.9	0.088	25.0	3.53

[a] Calculated from XRD, using Scherrer equation: $D = 0.89\ \lambda/(\beta \times \cos\theta)$.
[b] Calculated from BET, using $D = 6000/(\rho \times$ BET surface area), where $\rho = 3.79$ g cm^{-3} of anatase density.
[c] Porosity (%) = pore volume ($cm^3\ g^{-1}$)/(pore volume ($cm^3\ g^{-1}$) + solid catalyst volume without pore ($cm^3\ g^{-1}$)) × 100; the solid catalyst volume ($cm^3\ g^{-1}$) without pore was calculated from the density of anatase form (3.79 g cm^{-3}) and is equal to 1/density of the solid catalyst volume without pore.
[d] Based on Bragg's Law: $d = \lambda/(2 \times \sin\Theta)$, where $\lambda = 1.54$ Å.

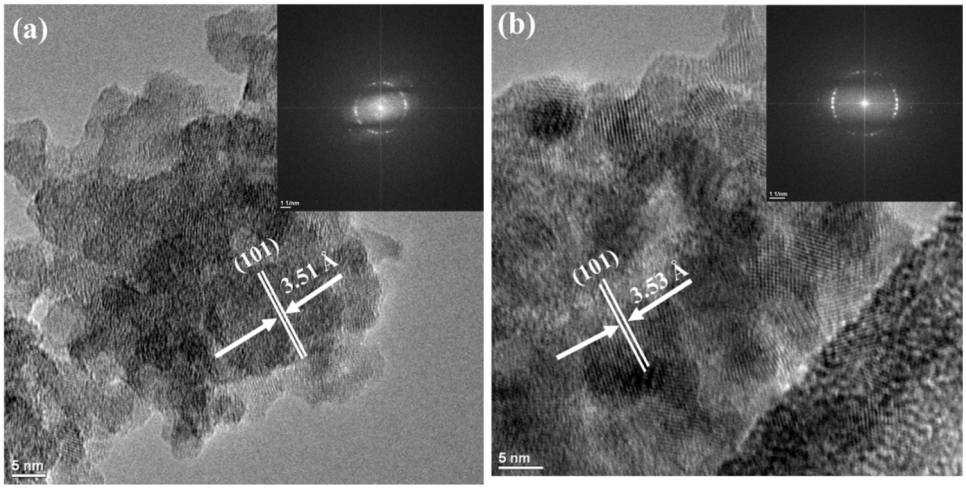

Fig. 4. High-resolution transmission electron microscopy images of (a) N-TiO_2 and (b) reference TiO_2 nanoparticles.

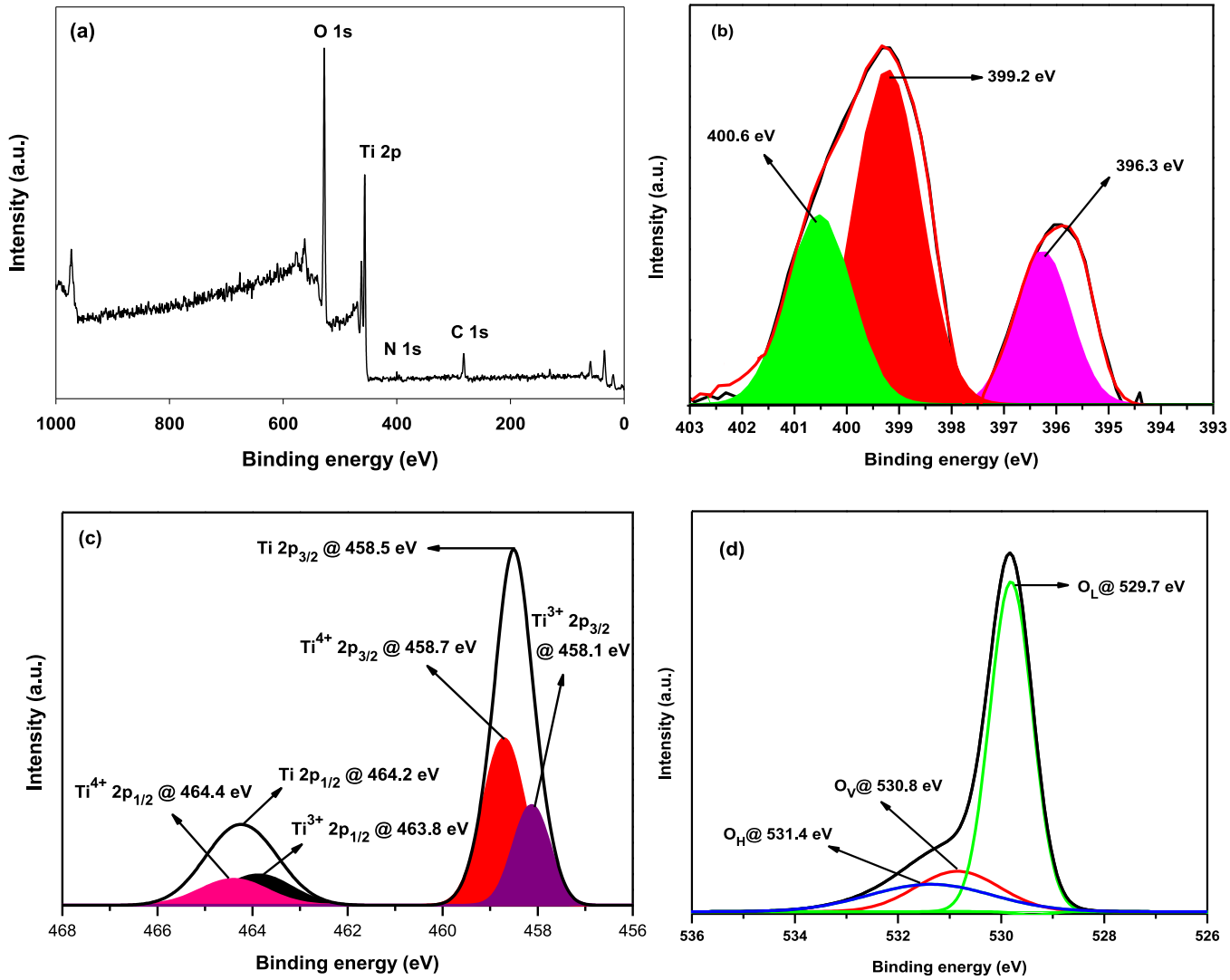

Fig. 5. (a) X-ray photoelectron spectroscopy (XPS) survey scan spectrum for N-TiO_2, (b) high resolution XPS spectrum of N 1 s core levels, (c) high resolution XPS spectrum of Ti 2p core levels, and (d) high resolution XPS spectrum of O 1 s levels.

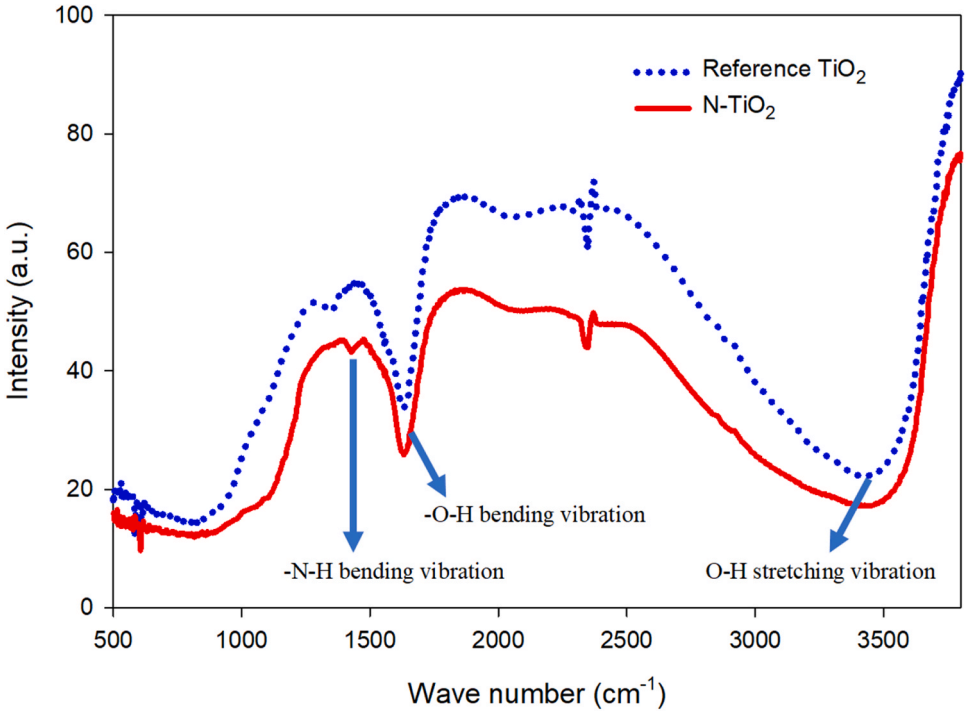

Fig. 6. Fourier transform infrared (FTIR) spectra of N-TiO_2 and reference TiO_2 nanoparticles.

[4]. Herein, the average crystallite sizes of N-TiO_2 and reference TiO_2 nanoparticles are calculated as 10.9 and 16.1 nm, respectively (Table 1).

HR-TEM was carried out for further investigation of the morphologies and crystal sizes of the N-TiO_2 and reference TiO_2 samples (Fig. 4). Analyzing the HR-TEM images, the average crystal sizes of the reference TiO_2 and N-TiO_2 samples were calculated as 15.8 ± 1.3 and 9.5 ± 0.9 nm, respectively. The results of HR-TEM are consistent with the XRD results. Moreover, lattice fringes having 3.51 and 3.53 Å as interlayer distances for the (101) planes of N-TiO_2 and reference TiO_2, respectively, were resolved in HR-TEM images. These results of interlayer distance of (101) planes are consistent with the results obtained from Bragg's equation (see Table 1). In addition, the morphologies of the prepared nanoparticles were also studied by fast Fourier transform (FFT). FFT patterns reveal clear rings for N-TiO_2 and reference TiO_2 nanoparticles indicating that these nanoparticles have one dominant crystal phase, i.e., anatase phase as revealed from XRD.

To identify the composition of N-TiO_2 and the nature of incorporated N-atoms in it, the N-TiO_2 sample was analyzed by XPS. In addition, the oxidation states of Ti and nature of O-atoms were also recognized by XPS analysis. Fig. 5a represents the spectrum of XPS survey scan of N-TiO_2. The spectrum of XPS survey scan of N-TiO_2 showed the occurrence of Ti, O, N and C, representing successful doping of N in N-TiO_2 samples. The peak at 284.5 eV has been previously assigned to C 1 s core level therefore, the detected C peak in the spectrum of XPS survey scan of N-TiO_2 possibly be due to the adventitious carbon atoms adsorbed on TiO_2 [49, 56]. The deconvoluted peaks for N 1 s core level in the high-resolution spectrum of N-TiO_2 were found at 396.3, 399.2 and 400.6 eV, characteristic peaks of the doped N (Fig. 5b) [41]. It is noteworthy to be mentioned here that the assignment of different XPS peaks detected for $N_{1\,s}$ core level in N-TiO_2 samples is still under debate. This is because, the nature of Ti and N precursors as well as the method of N-TiO_2 synthesis affect the position/energy of the XPS peaks of N 1 s core level. Various researchers have observed different XPS peaks, ranging from 396 to 404 eV, for $N_{1\,s}$ core level in N-TiO_2 samples and have assigned these peaks to either substitutional or interstitial state of nitrogen in N-TiO_2 lattice [24,49]. It has been reported that XPS peaks that appear at 396–397 eV are due to substitutional N-atoms and those which appear at about 400 eV are generally ascribed to interstitial nitrogen [24]. Analyzing the available XPS results of N-TiO_2 nanoparticles and comparing our results with the published data, we can conclude that the peaks detected at 396.3 and 399.2 eV in our work could be, respectively, attributed to substitutional and interstitial states of nitrogen in N-TiO_2 samples [24,25]. The peak at 400.6 eV could possibly be attributed to the surface adsorbed nitrogen species (essentially adsorbed NO_x) [41]. This peak (i.e., at 400.6 eV) could also be assigned to the interstitially doped nitrogen as reported by Zeng et al. [57]. Since both of the substitutional and interstitial states can induce localized energy states in the bandgap of TiO_2, we expect higher photocatalytic efficiency of the synthesized N-TiO_2 nanomaterials under visible light irradiation. The high-resolution spectrum of Ti 2p indicated two major peaks at binding energies of 458.5 and 464.2 eV (Fig. 5c). The former is assigned to Ti $2p_{3/2}$ and the later to Ti $2p_{1/2}$ [41,58]. Each of these two peaks were deconvoluted into two peaks, i.e., the peak at 458.5 eV into 458.1 and 458.7 eV; and the peak at 464.2 eV into 463.8 and 464.4 eV (Fig. 5c). The peaks at 458.1 and 463.8 eV are attributed to Ti^{3+} $2p_{3/2}$ and Ti^{3+} $2p_{1/2}$ states while the peaks at 458.7 and 464.4 eV are attributed to Ti^{4+} $2p_{3/2}$ and Ti^{3+} $2p_{1/2}$ states, respectively [58–60]. The existence of Ti^{3+} states show the presence of oxygen vacancies (O_V) in N-TiO_2. This is because, the reduction of Ti^{4+} to Ti^{3+} is accompanied by the formation of O_V for maintenance of electrostatic balance in accordance of reaction (5) [61].

$$4\,Ti^{4+} + O^{2-} \rightarrow 2\,Ti^{4+} + 2\,Ti^{3+} + \square + 0{\cdot}5\,O_2 \quad (5)$$

Where $\square$ indicates an empty position (vacancy) arising from the elimination of O^{2-} in the N-TiO_2 crystal lattice. Reaction (5) indicates, if not produced by other means, the ratio of Ti^{3+} to O_V will be 2:1in the lattice, as for each oxygen vacancy two Ti^{3+} are produced. The presence of Ti^{3+} in N-TiO_2 lattice is highly beneficial for the better activity of the photocatalyst since Ti^{3+} can suppress electron-hole recombination rate [58, 62]. Fig. 5d represents the full survey spectrum of O 1 s. This peak was fitted into three peaks at 529.7, 530.8 and 531.4 eV assigned to lattice oxygen (O_L), O_V, and hydroxyl groups adsorbed at the surface (O_H), respectively. The presence of O_V supports the claim that the existence of Ti^{3+} indirectly confirms the formation of O_V in the crystal lattice via

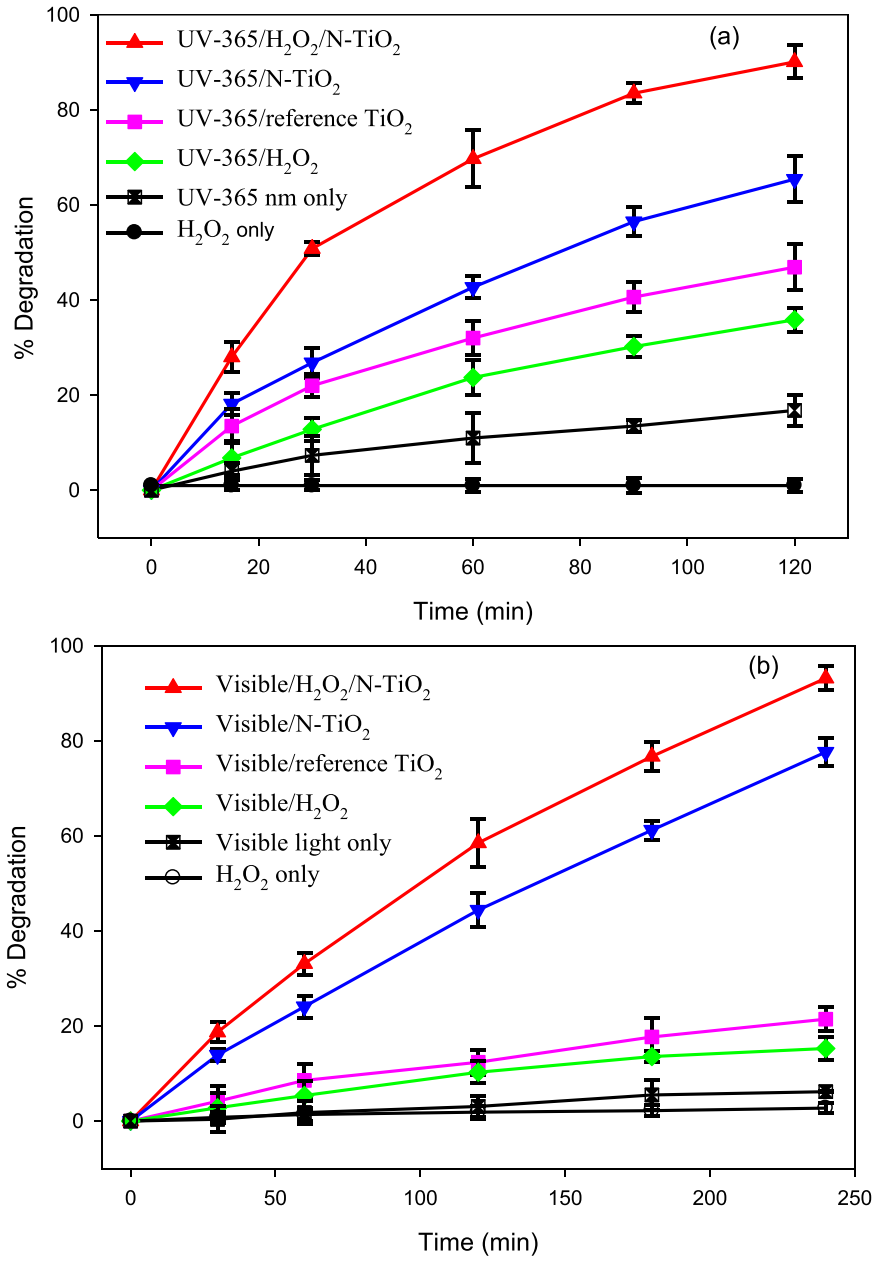

Fig. 7. Photocatalytic degradation of 2,4-DCP (a) under UV light irradiation and (b) under visible light irradiation. Reaction conditions: $[2,4\text{-DCP}]_0 = 153.4$ μM (25 mg/L), $[\text{catalyst}]_0 = 1$ g/L, $[H_2O_2]_0 = 2$ mM, pH = 5.6.

reaction (5). Similarly, to Ti^{3+}, O_V could also suppress the recombination rate of e^-/h^+ pairs by trapping the photogenerated electrons, thereby enhancing the photocatalytic activity of N-TiO_2 [58,62,63]. Moreover, O_V can boost the efficiency of photocatalysts via generation of superoxide radical anions ($O_2^{\bullet-}$) [23]. In addition, the efficiency of the N-TiO_2 nanoparticles can further be enhanced by O_H through production of hydroxyl radicals ($^{\bullet}OH$) by trapping holes (h^+) [58].

The FTIR spectra of reference TiO_2 and N-TiO_2 is given in Fig. 6. The broad band at 3439 cm^{-1} in both N-TiO_2 and reference TiO_2 is due to the stretching vibration of hydroxyl groups adsorbed at the surface of these materials [4,64]. The 1632 cm^{-1} band in both reference TiO_2 and N-TiO_2 samples is attributed to the bending vibration of water molecules adsorbed at the surface of photocatalysts [34]. The degree of TiO_2 hydroxylation greatly depends on the reaction conditions and methods of its synthesis. The hydroxyl groups adsorbed at the surface of photocatalysts has been reported to play a vital role in enhancing their photocatalytic activities. This is because, these hydroxyl groups transfer the photogenerated species during photocatalytic reaction thereby generating reactive species and lowers the recombination rate of electron-hole pairs. Another band at 1427 cm^{-1} was detected only in N-TiO_2 samples (Fig. 6). This band is due to the N-H bending vibration, revealing successful doping of N in TiO_2 crystal lattice [56,64].

3.2. Degradation of 2,4-dichlorophenol

To evaluate the photocatalytic efficiencies of reference TiO_2 and N-TiO_2 nanoparticles, 2,4-dichlorophenol (2,4-DCP) degradation was carried out under UV and visible light radiations. The results are presented in Fig. 7a-b. Only about 6% and 8% adsorption of 2,4-DCP on reference TiO_2 and N-TiO_2 have been observed after 120 min- which slightly increased to 7% and 10% at 240 min, respectively (data not shown). Thus, a very slight difference of 2,4-DCP adsorption on

reference TiO_2 and N-TiO_2 was found. Sole H_2O_2 and UV-365 nm light was capable of degrading only 1.90% and 16.8% 2,4-DCP, respectively, at 120 min of irradiation (Fig. 7a). However, in presence of H_2O_2 (2 mM) (i.e., UV-365/H_2O_2), the % degradation increased to 35.8%. The degradation of 2,4-DCP was promoted to 46.9% and 65.4%, respectively, while applying the UV-365/reference TiO_2 and UV-365/N-TiO_2 systems. Furthermore, combining the UV-365/N-TiO_2 with H_2O_2 (2 mM) (i.e., UV-365/H_2O_2/N-TiO_2), the degradation enhanced to 90.1% (Fig. 7a). The observed *pseudo-first-order* rate constant (k_{obs}) for sole H_2O_2, sole UV-365 nm light, UV-365/H_2O_2, UV-365/reference TiO_2, UV-365/N-TiO_2 and UV-365/H_2O_2/N-TiO_2 processes was calculated to be 0.0001, 0.0017, 0.0039, 0.0057, 0.0091 and 0.0203 min^{-1}, respectively (Fig. S1 (a) and (b), supporting information (SI)). Similarly, the degradation of 2,4-DCP, at 240 min of treatments, was calculated to be 2.76%, 6.2%, 15.3%, 21.5%, 77.6% and 93.1% by sole H_2O_2, sole visible light, visible/H_2O_2, visible/reference TiO_2, visible/N-TiO_2 and visible/H_2O_2/N-TiO_2, respectively (Fig. 7b). Whereas, the k_{obs} was found to be 0.0001, 0.0003, 0.0008, 0.0011, 0.0052 and 0.0078 min^{-1} for sole H_2O_2, sole visible light, visible/H_2O_2, visible/reference TiO_2, visible/N-TiO_2 and visible/H_2O_2/N-TiO_2, respectively (Fig. S1 (c) and (d), SI). These results suggest that UV-365 nm light is more effective in degrading 2,4-DCP than visible light. Moreover, higher photocatalytic performance of N-TiO_2 than reference TiO_2 was observed, possibly owing to the low bandgap of N-TiO_2. The photocatalytic activity difference, in terms of % degradation of 2,4-DCP, between N-TiO_2 and reference TiO_2 under UV-365 nm irradiation was calculated to be 18.5% (65.4%−46.9% = 18.5%). However, this activity difference increased to 56.1% (77.6%−21.5% = 56.1%) under visible light illumination. This activity difference could be due to the difference in the bandgap energies of reference TiO_2 and N-TiO_2. Since the bandgap energies of reference TiO_2 and N-TiO_2 were calculated to be 3.23 and 2.89 eV, respectively, visible light can activate N-TiO_2 but not reference TiO_2 whereas UV-365 nm radiation can activate both N-TiO_2 and reference TiO_2. It means that the visible light has activated the N-TiO_2 photocatalyst in visible/N-TiO_2 system and resulted in the production of reactive oxygen species (ROSs) such as $^{\bullet}OH$ and $O_2^{\bullet-}$ (reactions (5−8)) [4,65,66]. These ROSs then reacted with 2,4-DCP and resulted in its fast degradation (second-order rate constant between 2,4-DCP and $^{\bullet}OH$ is 7.4 (± 0.5) × 10^9 M^{-1} s^{-1}) (reaction (10)) [67]. Conversely, visible light was not capable of activating the reference TiO_2 and hence, very low degradation of 2,4-DCP (merely 21.5%) was obtained in visible/reference TiO_2 system. It is noteworthy to be mentioned here that this 21.5% degradation of 2,4-DCP by visible/reference TiO_2 system includes 7% 2,4-DCP adsorption on reference TiO_2 and 6.2% 2,4-DCP degradation by sole visible light (as explained above). Hence, the visible light based photocatalysis of reference TiO_2 (visible/reference TiO_2 photocatalysis) contributed to 8.3% (21.5%−(7%+6.2%) = 8.3%) degradation of 2,4-DCP. However, in reality the visible light is not capable of degrading 2,4-DCP directly as well as not capable of TiO_2 activation to generate reactive radicals which could lead to 2,4-DCP degradation. Thus, the observed photolysis (6.2%) and photocatalysis by visible/reference TiO_2 (8.3%) of 2,4-DCP could be due to some UV radiations- albeit with low intensity- which possibly enter the reaction solution along with visible light. The possible presence of UV radiations suggested that UV block filter may not completely eliminate/block the UV portion of the lamp and some UV radiations still enter the solution.

$$2N - TiO_2 \xrightarrow{UV/visible} h_b^+ + e_{cb}^- \quad (6)$$

$$H_2O_{ads} + h_{vb}^+ \rightarrow {}^{\bullet}OH + H^+ \quad (7)$$

$$OH^- + h_{vb}^+ \rightarrow {}^{\bullet}OH \quad (8)$$

$$O_2 + e_{cb}^- \rightarrow O_2^{\bullet-} \quad (9)$$

$$2,4 - DCP + {}^{\bullet}OH, O_2^{\bullet-} \rightarrow CO_2^{\bullet-} + H_2O + Cl^- \quad (10)$$

Similarly, the difference in % degradation of 2,4-DCP between UV-365/H_2O_2/N-TiO_2 and UV-365/N-TiO_2 systems was 24.7% (90.1% − 65.4% = 24.7%) whereas this difference was found to be 15.5% (93.1% − 77.6% = 15.5%) between visible/H_2O_2/N-TiO_2 and visible/N-TiO_2 systems. It means that H_2O_2 played more positive role in photocatalytic process based on UV-365 nm light than the one based on visible light. The higher synergetic role of H_2O_2 in UV-365/H_2O_2/N-TiO_2 system is because of the dual activation of H_2O_2 in this system, i.e., (i) activation by UV-365 nm radiation and (ii) activation by photocatalytically produced e_{cb}^-/$O_2^{\bullet-}$ (reactions (10−12)) [4,68–72]. On the other hand, only single activation of H_2O_2 available in visible/H_2O_2/N-TiO_2 system, i.e., activation by photo-catalytically produced e_{cb}^-/$O_2^{\bullet-}$ only and not by light (because visible light is not capable by activating H_2O_2).

$$H_2O_2 \xrightarrow{UV} 2{}^{\bullet}OH \quad (11)$$

$$H_2O_2 + O_2^{\bullet-} \rightarrow OH^- + {}^{\bullet}OH + O_2 \quad (12)$$

$$H_2O_2 + e_{cb}^- \rightarrow OH^- + {}^{\bullet}OH \quad (13)$$

By increasing the treatment time of the visible/N-TiO_2 system, a continuous reduction in the 2,4-DCP concentration was observed, leading to 100% degradation at 420 min

3.3. Identification of reactive species and degradation products

Since visible/N-TiO_2 system is economically more feasible process, this system was further evaluated. It had been found that the degradation/removal of organic substances in photocatalysis is carried out by photo-catalytically produced ROSs such as $^{\bullet}OH$, e_{cb}^-, h^+, H_2O_2 and $O_2^{\bullet-}$ [66,73–76]. However, the relative contribution of each ROS generally depends on the type of organic pollutant/compound and on the photocatalytic system. To explore the relative contribution of different possible ROSs towards 2,4-DCP degradation, quenching experiments were conducted by applying specific scavengers of these ROSs. The specific scavengers used in this study were: (i) iso-propanol (*i*-PrOH) for quenching $^{\bullet}OH$; (ii) methanol (MeOH) for scavenging $^{\bullet}OH$ and h^+; (iii) Fe(II)-EDTA for H_2O_2; and (iv) potassium dichromate ($K_2Cr_2O_7$) for e_{cb}^-.

Table 2
k_{obs} and % reduction in k_{obs} of photocatalytic degradation of 2,4-DCP in the presence of different scavengers. Experimental conditions: $[2,4\text{-DCP}]_0$ = 153.4 μM (25 mg/L), $[N\text{-}TiO_2]_0$ = 1 g/L, $[MeOH]_0$ = $[i\text{-PrOH}]_0$ = 100 mM, $[Fe(II)\text{-EDTA}]_0$ = 10 μM, $[K_2Cr_2O_7]_0$ = 50 μM.

Experimental condition	Purpose	k_{obs} (min^{-1})	% Reduction in k_{obs}
No scavenger	———	0.0052	———
MeOH	To scavenge $^{\bullet}OH$ and h^+	0.0022	57.7
i-PrOH	To scavenge $^{\bullet}OH$	0.0024	53.8
Fe(II)-EDTA	To scavenge H_2O_2	0.0048	7.7
$K_2Cr_2O_7$	To scavenge e^-	0.0034	34.6
1,4-Benzoquinone (*p*-BQ)	To scavenge $O_2^{\bullet-}$	0.0037	28.8
MeOH + N_2 saturation	To scavenge h^+ and $^{\bullet}OH$ and eliminates the formation of $O_2^{\bullet-}$	0.0008	84.6
MeOH + O_2 saturation	To scavenge h^+ and $^{\bullet}OH$ and promotes the formation of $O_2^{\bullet-}$	0.0025	51.9

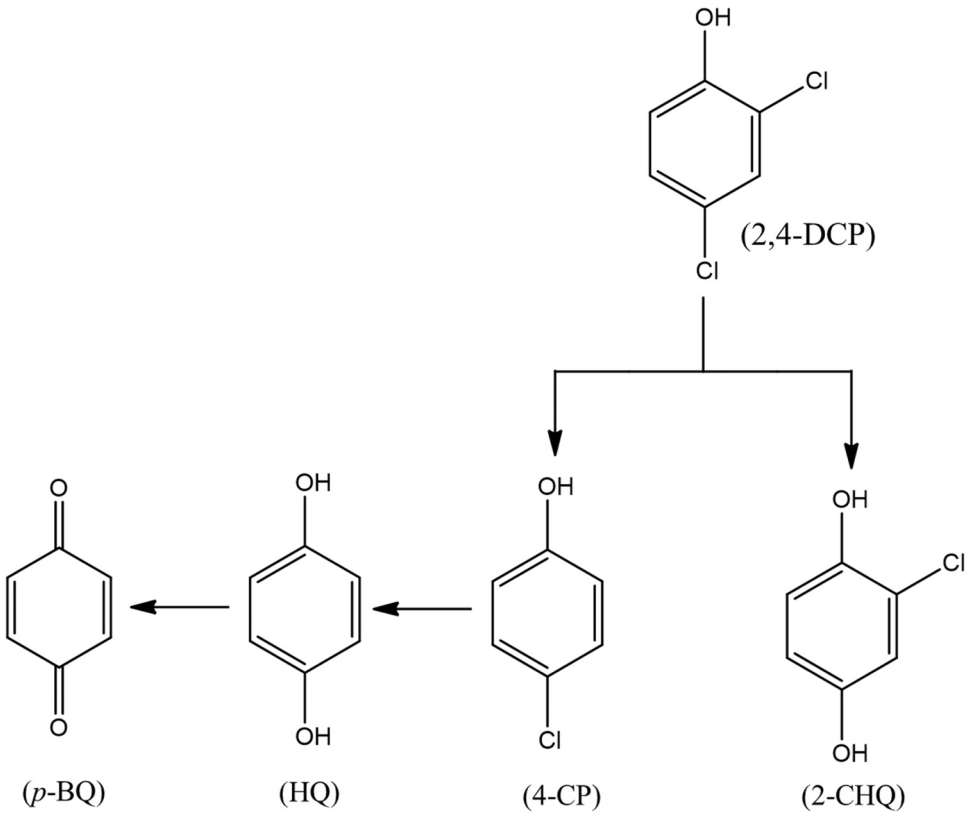

Scheme 1. Degradation products and pathways of 2,4-DCP by visible/N-TiO_2 system.

The results are presented in Table 2. The observed rate constant (k_{obs}), based on *pseudo-first-order* kinetics, was calculated as 0.0052 min^{-1} in absence of scavenger. By applying MeOH and *i*-PrOH as specific scavengers, the k_{obs} decreased to 0.0022 (reduction in k_{obs} = (0.0052 −0.0022)/0.0052 × 100 = 57.7%) and 0.0024 (reduction in k_{obs} = (0.0052 −0.0024)/0.0052 × 100 = 53.8%) min^{-1}, respectively. These results demonstrated that the relative contribution of •OH towards degradation of 2,4-DCP was 53.8% (reduction obtained in presence of *i*-PrOH (•OH scavenger) and that of h^+ was 3.9% (57.7%–53.8% = 3.8%, difference between MeOH and *i*-PrOH). It is noteworthy to be mentioned here that 3.9% contribution of h^+ represents the direct contribution of h^+ towards 2,4-DCP degradation, possibly through electron transfer reaction, else the credit of •OH contribution towards 2,4-DCP degradation also goes to h^+ since these are the h^+ which are

Table 3
% Degradation of 2,4-DCP, percent relative inhibition (INH%) of bioluminescence of *Vibrio fischeri* by 2,4-DCP treated solutions, % removal of TOC and concentration of chloride ion formation during photocatalytic degradation of 2,4-DCP by visible/N-TiO_2 system. Experimental conditions: $[2,4\text{-DCP}]_0$ = 153.4 μM, $[\text{N-TiO}_2]_0$ = 1 g/L, pH = 5.6.

Treatment time (min)	% Degradation of 2,4-DCP	INH%	% Removal of TOC	Chloride formation (μM)
0	0.0	68	0	0
60	24.1	70	6.3	33.5
120	44.4	76	13.4	62.8
180	61.2	82	21.6	98.8
240	77.6	87	32.2	133.4
300	89.8	89	43.3	166.9
360	97.8	81	55.5	195.6
420	100.0	52	65.8	215.8
480	100.0	26	73.8	234.5
540	100.0	12	80.5	248.2

Table 4
Aquatic toxicity of 2,4-DCP and its detected DPs (all values are in units of mg L^{-1}).

Compound	Acute Toxicity			Chronic Toxicity		
	Fish (LC_{50})	Daphina (LC_{50})	Green Algae (EC_{50})	Fish (ChV)	Daphina (ChV)	Green Algae (ChV)
2,4-DCP	25.5	15.6	15.8	2.72	1.87	4.87
2-CHQ	232.0	128.0	84.0	21.9	11.5	20.6
4-CP	67.3	43.9	34.8	7.59	4.46	9.40
HQ	669	347	179	58.8	26.4	38.4
p-BQ	3.33×10^3	1.61×10^3	614	269	100	112

responsible for $^{\bullet}OH$ formation via reactions (7) and (8). When Fe (II)-EDTA was used as a scavenger, a 7.7% reduction in k_{obs} was noted (k_{obs} reduced from 0.0052 to 0.0048 min^{-1}, Table 2) indicating that either H_2O_2 played a minor role in 2,4-DCP degradation or a negligible amount of H_2O_2 was produced in the visible/N-TiO_2 system. When H^+ ions are present in the reaction solution, $O_2^{\bullet-}$ could lead to the formation of H_2O_2 through reaction (13) [4].

$$O_2^{\bullet-} + 2\,H^+ + e_{cb}^- \rightarrow H_2O_2 \quad (14)$$

Since we had performed the photocatalytic experiments at pH 5.6 (unadjusted), we expect that a negligible amount of H_2O_2 was produced in the visible/N-TiO_2 system. Table 2 also shows a 34.6% reduction in k_{obs}, as it reduced from 0.0052 to 0.0034 min^{-1}, when $K_2Cr_2O_7$ was added to visible/N-TiO_2 system as e_{cb}^- scavenger. To further evaluate the direct and indirect contribution of e_{cb}^- (i.e., via formation of $O_2^{\bullet-}$ (reaction (9))) towards 2,4-DCP degradation, experiments in the occurrence of 1,4-benzoquinone (*p*-BQ), MeOH + N_2 saturation, and MeOH + O_2 saturation were performed. *p*-BQ scavenges $O_2^{\bullet-}$, MeOH + N_2 can scavenge h^+ and $^{\bullet}OH$ as well as eliminates the formation of $O_2^{\bullet-}$ thereby allows only e_{cb}^- in the photocatalytic system to attack 2,4-DCP, and MeOH + O_2 can scavenge h^+ and $^{\bullet}OH$ as well as promotes the formation of $O_2^{\bullet-}$ (via reaction (9)) thereby allows $O_2^{\bullet-}$ and e_{cb}^- (non-reacted with O_2) in the photocatalytic system to attack 2,4-DCP. The results exhibited that *p*-BQ has reduced the k_{obs} by 28.8% (i.e., from 0.0052 to 0.0037 min^{-1}) (Table 2), indicating 28.8% contribution from $O_2^{\bullet-}$.

Similarly, the reduction in k_{obs} was calculated to 84.6% (i.e., from 0.0052 to 0.0008 min^{-1}) in MeOH containing system saturated with N_2, showing 15.4% contribution of e_{cb}^- towards degradation of 2,4-DCP (Table 2). These results indicated that the reduction caused by $K_2Cr_2O_7$ (e_{cb}^- scavenger) was due to the suppression of $O_2^{\bullet-}$ formation due to the scavenging of e_{cb}^-. The reduction caused by MeOH + N_2 (i.e., 84.6%) was close to the total reduction caused by MeOH and *p*-BQ, i.e., 86.5% (57.7% by MeOH and 28.8% by *p*-BQ). This is because, both systems develop similar situations, i.e., eliminate $^{\bullet}OH$, h^+ and $O_2^{\bullet-}$ from the reaction solutions. To further confirm the involvement of $O_2^{\bullet-}$ in the degradation of 2,4-DCP by visible/N-TiO_2 system, experiments were conducted in the presence of MeOH saturated with O_2. In presence of MeOH + O_2 system, the k_{obs} decreased from 0.0052 to 0.0025 min^{-1}, i.e., 51.9% reduction. This reduction is less than that observed in MeOH containing solution (i.e., 57.7%). Thus, it suggests that a relatively high level of $O_2^{\bullet-}$ was produced when the solution was saturated with O_2 gas than in non-saturated (ordinary) solution. As a result, higher degradation of 2,4-DCP was found in MeOH + O_2 system which further confirms the participation of $O_2^{\bullet-}$ in the degradation of 2,4-DCP.

To elucidate the possible pathways of 2,4-DCP photocatalytic degradation by visible/N-TiO_2, the degradation products (DPs) were identified by GC-MS. A total of four DPs were identified in the present study, namely 4-chlorophenol (4-CP), 2-chlorohydroquinone (2-CHQ), hydroquinone (HQ) and 1,4-benzoquinone (*p*-BQ), shown in Scheme 1. The GC-MS spectra of these detected by-products are given in Fig. S2, supporting information (SI). All of the DPs, identified in this study, were previously detected by other researchers in 2,4-DCP degradation studies by different AOPs [44,77–79]. Although many researchers have identified 4-CP as one of the DPs of 2,4-DCP, yet its precise mechanism of formation is still not clear. On the basis of different reactive species (i.e., e_{cb}^-, h_{vb}^+, H^+ and $O_2^{\bullet-}$) present in the photocatalytic system (produced via reactions (6), (7) and (9)), we are proposing the following pathway of 4-CP formation from 2,4-DCP (reaction (15)) [80,81]. Thus, 2,4-DCP could produce 4-CP via de-chlorination followed by hydrogenation reactions, shown in reaction (15).

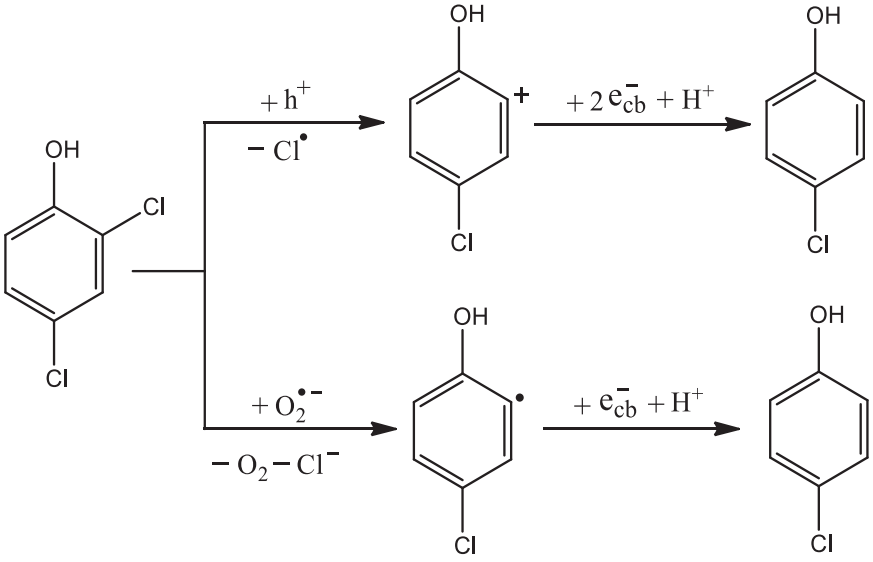

(15)

Dechlorination-hydroxylation of 2,4-DCP could lead to the formation of 2-CHQ as its DP, possibly through three different routes (reaction (15)) [78]. Similarly, this type of dechlorination-hydroxylation reaction of 4-CP could lead to the formation of HQ, also shown in reaction (16), in brackets.

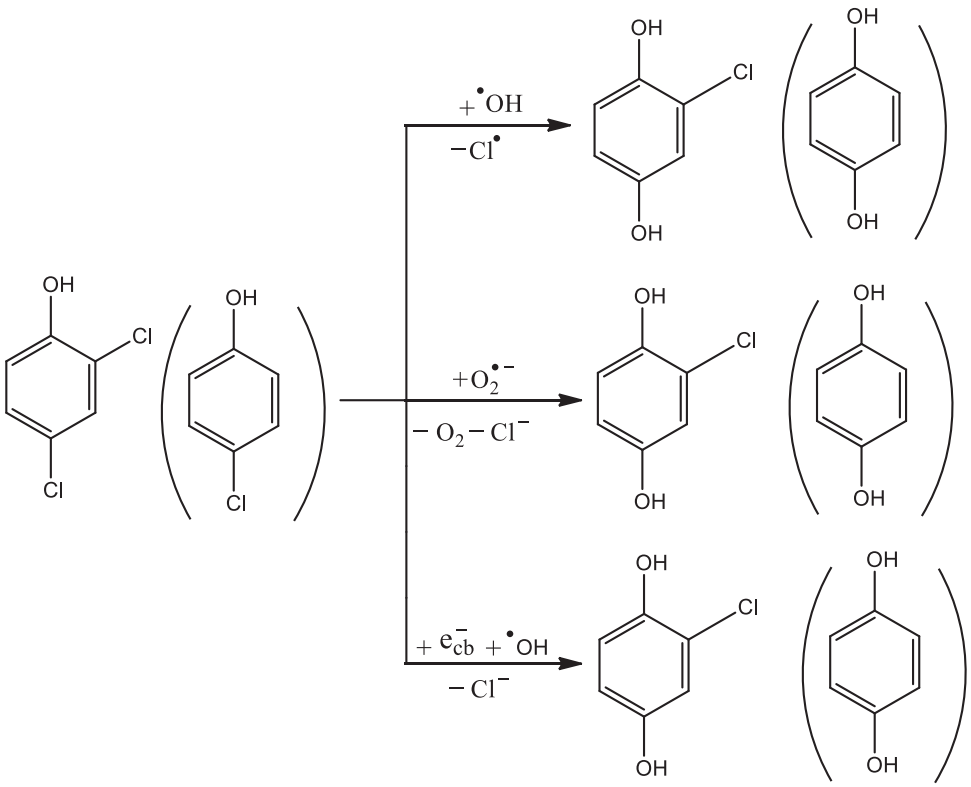

(16)

Hydrogen abstraction from HQ by •OH led to the production of *p*-BQ (reaction (17)), as also suggested by Shi et al. [77] and Wang et al. [78].

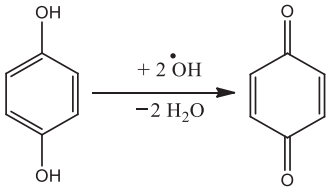

(17)

A total of four DPs were identified in the present study, namely 4-chlorophenol (4-CP), 2-chlorohydroquinone (2-CHQ), hydroquinone (HQ) and 1,4-benzoquinone (*p*-BQ), shown in Scheme 1.

The detected DPs were quantified to confirm whether the visible/N-TiO_2 system is capable of degrading the DPs of 2,4-DCP or not. The quantification of the detected DPs during the course of treatment provides useful information about the toxicity of the photo-catalytically treated solution. This is because, the DPs are sometimes more noxious/harmful than the parent compound. Thus, in such a scenario, the elimination of DPs is highly necessary for reducing the toxicity of treated waters. In case, of 2,4-DCP degradation, the DPs such as HQ and *p*-BQ have been reported to be more toxic than 2,4-DCP itself. Therefore, the quantification of these two products is essential to test the practical applicability of the visible/N-TiO_2 system for real water treatments. To achieve the complete degradation of 2,4-DCP and its toxic DPs from treated waters, the treatment time was increased to 540 min. The quantification results show that 4-CP and 4-CHQ initially accumulated in the treated solution up to 17.8 and 11.4 μM, respectively, at 240 min of treatment time. The remaining concentration of 2,4-DCP at 240 min of treatment was 34.4 μM (77.6% was degraded). However, the concentration of 4-CP and 4-CHQ was observed to decrease on further irradiation and reached to 12.1, 4.3 and 0.0 μM for 4-CP and 8.6, 2.4 and 0.0 μM for 4-CHQ at reaction time of 300, 360 and 420 min, respectively. Analogous trends were found for HQ and *p*-BQ. The concentration of HQ reached to a maximum value of 14.3 μM at 300 min of treatment time whereas that of *p*-BQ reached to 15.2 μM at treatment time of 360 min. Luckily, a decline in the concentration of both HQ and *p*-BQ were observed at 420 min of treatment, i.e., 4.5 μM for HQ and 8.1 for μM *p*-BQ.

According to molar balance data calculations, 56.5%, 52.6%, and 50.8% of the 2,4-DCP was transformed to 4-CP, 4-CHQ, HQ and *p*-BQ at 60, 120 and 180 min of the treatment time, respectively (Fig. S3 and Table S1). On prolong treatment, the share of these four DPs (i.e., 4-CP, 4-CHQ, HQ and *p*-BQ) to total DPs of 2,4-DCP reduces to 42.3%, 35.0%, 21.8%, 8.2%, 1.8% and 0.0% at reaction time of 240, 300, 360, 420, 480 and 540 min, respectively (Fig. S3 and Table S1). The continuous reduction in the concentration of the detected DPs with treatment time indicated that these DPs further converted to small organic acid molecules and finally to H_2O and CO_2 as evidenced from the mineralization study which exhibited ceaseless abatement with the reaction time (See Section 3.4).

3.4. Toxicity evaluation and degree of mineralization and de-chlorination

It is highly important to achieve a higher degree of toxicity reduction while dealing with the degradation/removal of toxic organic compounds/pollutants. Therefore, to evaluate the possibility of practical applications of visible/N-TiO_2 system, the toxicity changes during the photocatalytic treatment of 2,4-DCP were measured. Generally, organic compounds are more toxic than the inorganic products/ions produced by these organic compounds upon decomposition. Therefore, the removal of TOC during the 2,4-DCP photocatalytic degradation was also assessed. Moreover, the chloride removal efficiency was also measured in this study since the rate of de-chlorination of 2,4-DCP has been reported to be an important indicator of toxicity reduction [44]. To achieve higher level of toxicity reduction and TOC removal, the treatment time was increased to 540 min, as in case of DPs quantification. The overall results of toxicity changes, removal of TOC and Cl^- formation are represented in Table 3.

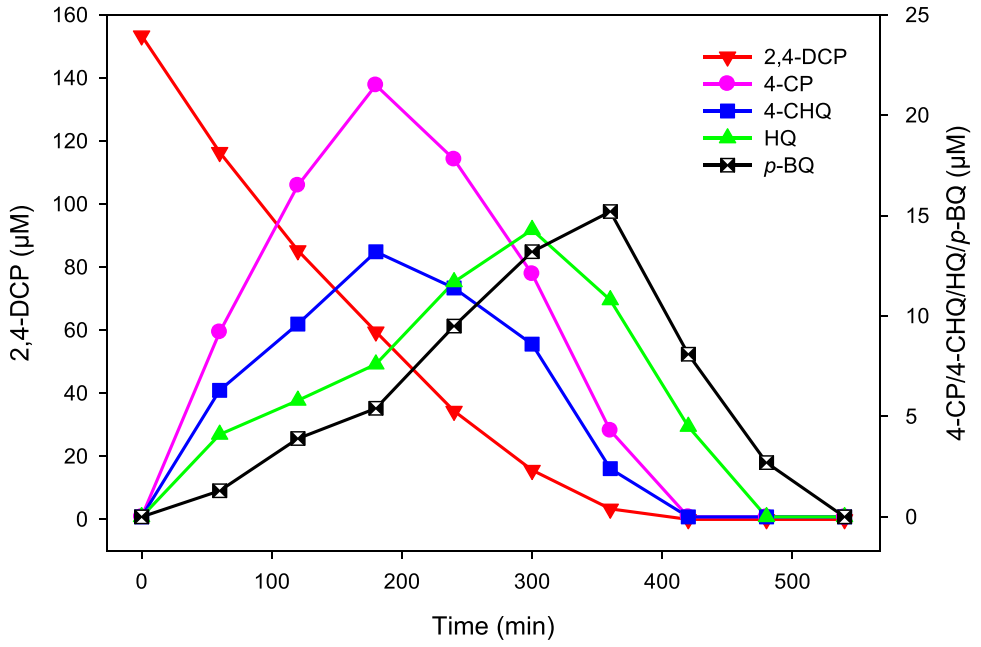

Fig. 8. Decay of 2,4-DCP and formation and decay of 4-CP, 4-CHQ, HQ and *p*-BQ by visible/N-TiO_2 system. Reaction conditions: $[2,4\text{-DCP}]_0 = 153.4$ μM, $[\text{catalyst}]_0 = 1$ g/L. pH = 5.6.

Complete (100%) degradation of 2,4-DCP was achieved at 420 min of treatment time (Table 3). The acute toxicity changes did not follow the trend of 2,4-DCP degradation with treatment time, i.e., with the reduction in 2,4-DCP concentration, no parallel reduction in toxicity was observed. Rather, an increase in acute toxicity was observed from 68% INH at 0 min of treatment to 89% INH at 300 min of treatment. This increase in toxicity could be due to the harmful products of 2,4-DCP such as 4-CP, 4-CHQ, HQ and *p*-BQ. Previously, the EC_{50} values for 2,4-DCP, 4-CP, HQ and *p*-BQ were reported to be 2.4, 1.2, 0.088 and 0.035 mg/L, respectively, indicating toxicity order of these compounds as: *p*-BQ > HQ > 4-CP > 2, 4-DCP. Thus, the increase in toxicity at the early stages of the experiment could possibly be ascribed to the toxic DPs produced in the system. Luckily, on prolong treatment, the toxicity has been found to reduce continuously, reaching 12% INH at 540 min of treatment. The overall toxicity reduction was 82.4% ((68−12)/68 × 100)- calculated from 68% INH at 0 min and 12% INH at 540 min of treatment. The reduction in toxicity on prolong treatment suggest that the DPs were later degraded by the photocatalytic system.

The degradation of 2,4-DCP and its DPs on prolong treatment could be confirmed from the removal of TOC. The removal of TOC was found to be 80.5% at 540 min of treatment, suggesting the destruction of organic compounds, i.e., 2,4-DCP and its DPs. Consequently, toxicity reduced with the degradation of organic compounds, indicating the higher hazardous nature of these organic compounds as compared to their inorganic counterparts. Furthermore, the Cl^{-1} concentration increased from 0 μM at 0 min to 248.2 μM at 540 min, indicating the de-chlorination of 2,4-DCP and its DPs. Since the de-chlorination of phenolic compounds has been associated with toxicity reduction (e.g., phenol has lower toxicity than 2,4-DCP), reduced toxicity has been observed at higher treatment time. The theoretical calculations shows that 153.4 μM 2,4-DCP could produce 306.8 μM Cl^{-1} (because one molecule of 2,4-DCP contains 2 Cl atoms). Thus, the mass balance data indicated that 80.9% (248.2 μM/306.8 μM ×100 = 80.9%) of chlorine could be removed as Cl^{-1} from 2,4-DCP and its DPs at 540 min of treatment time.

To further assess the toxicity of the parent 2,4-DCP and its detected DPs- ECOSAR- toxicity assessing software- was used [45]. The results obtained are presented in Table 4. It can be seen that 2,4-DCP is more toxic than all the detected DPs (2-CHQ, 4-CP, *p*-BQ and HQ) towards the three aquatic organisms namely fish, daphnia and green algae in terms of both acute and chronic toxicities. It means that conversion of 2,4-DCP to its DPs resulted in the decrease of the toxicity of the 2,4-DCP treated solution towards these aquatic organisms. Since 2,4-DCP continuously decreased in the solution, a similar trend could be expected in toxicity reduction (linear) with treatment time. Thus, the visible/N-TiO_2 system is supposed to be an environmentally friendly technology that not only eliminated the 2,4-DCP but also led to the toxicity reduction of the treated solution. Of note, these results are contrary to the experimental results of the INH% of bioluminescence of *Vibrio fischeri* by 2,4-DCP treated solution where initially an increase and then a decrease in toxicity was observed. The possible explanation for this contrary observation is that: either the identified DPs of 2,4-DCP are more toxic towards *Vibrio fischeri* and less toxic towards fish, daphnia and green algae than 2,4-DCP itself or there might be some toxic products of 2, 4-DCP which are produced in the treated solution but in so much less quantity that is beyond the limit of GC-MS detection.

3.5. Evaluation of photocatalytic activity for hydrogen production

To achieve the higher energy demands, especially of the energy-deficient countries such as Pakistan, new renewable energy resources should be discovered. In this regard, hydrogen (H_2) formation from water splitting or photo-reforming of methanol/ethanol by means of a visible light active photocatalyst and natural sun light energy is one of the best alternatives to the energy obtained from contaminative and diminishing fossil fuels. To realize this desirable objective of green energy synthesis, the prepared N-TiO_2 nanoparticles were tested for H_2 formation via water splitting/photo-reforming of methanol. Neither N-TiO_2 nanoparticles nor the light emitted by 300 W Xe lamp was capable of H_2 production, i.e., no H_2 was produced in the control experiments. Thus, the H_2 production from water, as found in this study, could be considered to be a purely photo-catalyzed reaction. In this type of photo-catalyzed reaction, the holes of the valence band of the photocatalyst undergo oxidation by water or sacrificial agent (methanol in this study) molecules leading to the formation of H^+ (reaction (18)) [82]. The electron of the conduction band reduces the H^+ thereby generating H_2 gas (reaction (19)) and hence, complete the cycle of H_2 formation via water splitting/photo-reforming [82].

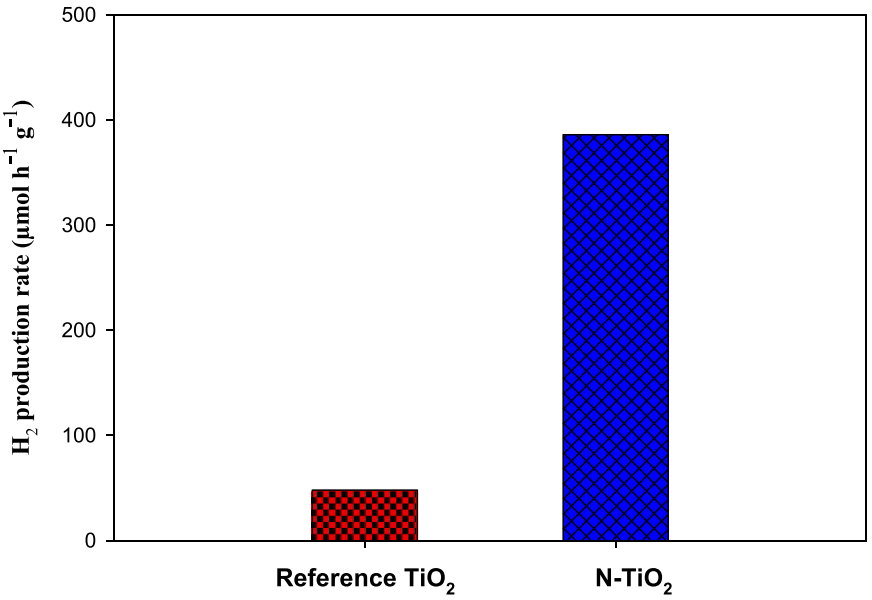

Fig. 9. Rate of H_2 production by reference TiO_2 and N-TiO_2 nanoparticles under visible light irradiation from a 300 W Xe arc lamp in 100 mL of 20 vol% aqueous methanol solution. Reaction conditions: $[catalyst]_0 = 1$ g/L, $[co\text{-}catalyst]_0 = 0.2$ wt% Pt, pH = 5.6.

$$h^+ + H_2O/CH_3OH \rightarrow {}^{\bullet}OH,\ CO_2,\ H^+ \quad (18)$$

$$2\ H^+ + 2\ e^- \rightarrow H_2 \quad (19)$$

The reference TiO_2 nanoparticles were found to have very low activity for H_2 production. For reference TiO_2, the rate of H_2 production was calculated to be 48 μmol h^{-1} g^{-1} (Fig. 8). The lower activity of reference TiO_2 nanoparticles could possibly be due to the large bandgap energy, little or no activation by visible light and possibly fast electron-hole pair recombination. However, the observed limited photocatalytic H_2 production activity (i.e., 48 μmol h^{-1} g^{-1}) of reference TiO_2 could be due to the activation of reference TiO_2 by the UV radiations which could possibly enter the reaction solution along with visible light (due to the possible ineffectiveness of the UV block filter to 100% filter out the UV radiations, as discussed in Section 3.2 in detail). Fortunately, H_2 formation rate was significantly enhanced to 386 μmol h^{-1} g^{-1} when N-TiO_2 nanoparticles were used (Fig. 8). The higher activity of N-TiO_2 nanoparticles for H_2 production could possibly be attributed to its lower bandgap energy and higher activation by visible light (as explained in detail in Section 3.1). Previously, H_2 production rate of 38, 120, 211, 670, 570, 865 and 19848 μmol h^{-1} g^{-1} have reported for nitrogen doped TiO_2 nanoparticles by different researchers [34,41,83–86]. The variation in H_2 production rate in different studies could mainly be attributed to the different type of methods of N-TiO_2 synthesis as well as other experimental conditions such as the uses of different light (irradiation) sources and sacrificial agents, the presence/absence of a cocatalyst in the reaction mixture, and so on.

The AQE of H_2 production of N-TiO_2 samples (in presence of 0.2 wt% Pt as co-catalyst) was calculated to be 3.9% at 360 nm. This AQE was found to be greater than the AQE of Pt-loaded TiO_2 which was calculated to be < 1% at 360 nm [87]. However, the calculated AQE was about 61.9% and 40.2% of the AQEs calculated for MoS_2/TiO_2 (AQE = 6.4% at 360 nm) [42] and MoS_2-graphene/TiO_2 (AQE = 9.7% at 365 nm) [88], respectively. However, for Pt or Pd loaded N-TiO_2, different values of AQE had been reported such as 3.7% at 420 nm for 0.5 wt% Pt loaded on N-TiO_2 [84], 5.3% at 365 nm and 10.6% at 312 nm for 1 wt% Pt loaded on N-TiO_2 [89], and 5.6% at 540 nm for 0.5 wt% Pd loaded on N-TiO_2 [90]. It can be concluded from these results that the synthesis of visible light responsive noble-metal-free photocatalysts such as N-TiO_2 is a feasible choice for water splitting to generate green energy in the form of H_2. This study showed that economically affordable materials- capable of activation by natural sun light- should be investigated as cost-effective water treatment and renewable energy production technologies. .

3.6. Environmental implications

The visible/N-TiO_2 photocatalytic system is supposed to be a cost-efficient process for achieving environmental sustainability in terms of water purification and green energy production. This system utilizes visible light- which is freely and ceaselessly available in the form of natural solar light- and TiO_2- a cheap and non-toxic semiconductor. Thus, if realize the goals of effective degradation of organic contaminants and hydrogen production at large scale via visible/N-TiO_2 system, a control over the waterborne diseases and the fulfillment of higher energy demands could be achieved. Daily, aquatic environment receives huge amount of chlorinated organic compounds (COCs) from industries, agricultural lands, hospitals, households, and animal husbandries. These COCs are considered to be toxic and their toxicity is primarily owing to the occurrence of chlorine [91,92]. Thus, the removal chlorine atom from these compounds could possibly reduce the toxicity of treated water. Since we have observed the de-chlorination of 2,4-DCP in the visible/N-TiO_2 system, the present work suggest that this system could be used for water detoxification containing COCs.

4. Conclusion

Visible light responsive N-TiO_2 photocatalyst was successfully synthesized by a modified sol-gel method. Nitrogen doping improved the properties of TiO_2, e.g., the BET surface area of TiO_2 was increased from 83.6 m^2/g (reference TiO_2) to 131.8 m^2/g (N-TiO_2). The bandgap energies of 2.89 and 3.23 eV were found for N-TiO_2 and reference TiO_2 samples, respectively. N-TiO_2 nanoparticles showed higher efficiency than reference TiO_2 under UV as well as visible light irradiation. Although, the degradation rate of 2,4-DCP by N-TiO_2 nanoparticles was higher under UV light irradiation than visible light, prolonged treatment of 2,4-DCP by visible/N-TiO_2 system led to 100% degradation of 2,4-DCP with more than 80% reduction in TOC. Addition of H_2O_2 (2 mM) accelerated the degradation efficiency of 2,4-DCP from 77.6% to 93.1% at 240 min by visible/N-TiO_2 system. The mechanistic studies revealed the participation of h^+_{vb}, e^-_{cb}, ${}^{\bullet}OH$ and $O_2^{\bullet -}$ in the degradation of 2,4-DCP

by visible/N-TiO_2 system, although by different extent. Four degradation products of 2,4-DCP were observed, namely 4-chlorophenol, 2-chlorohydroquinone, hydroquinone and 1,4-benzoquinone. More interestingly, visible/N-TiO_2 system, with 0.2 wt% Pt co-catalyst, was found to be capable of H_2 production from aqueous methanol solution at the rate of 386 μmol h^{-1} g^{-1} and AQE of 3.9% at 360 nm light. The study revealed that affordable water treatment and green energy production technologies should be explored for obtaining environmental sustainability.

CRediT authorship contribution statement

Javed Ali Khan: Conceptualization, Data curation, Formal analysis, Investigation, Methodology, Writing – original draft. **Murtaza Sayed:** Conceptualization, Data curation, Formal analysis, Investigation, Methodology, Resources, Writing – original draft. **Noor S. Shah:** Conceptualization, Project administration, Supervision, Funding acquisition, Validation, Writing – review & editing. **Sanaullah Khan:** Software, Validation, Writing – review & editing. **Ashfaq Ahmad Khan:** Conceptualization, Writing – review & editing. **Muhammad Sultan:** Conceptualization, Writing – review & editing. **Ammar M. Tighezza:** Writing – review & editing. **Jibran Iqbal:** Writing – review & editing. **Grzegorz Boczkaj:** Conceptualization, Writing – review & editing.

Declaration of Competing Interest

The authors declare that they have no known competing financial interests or personal relationships that could have appeared to influence the work reported in this paper.

Data Availability

Data will be made available on request.

Acknowledgments

Higher Education Commission (HEC), Pakistan, is highly acknowledged for financial support through National Research Program for Universities (NRPU) Project, Ref No. 20-15851/NRPU/R&D/HEC/2021–2020. Ammar M. Tighezza is grateful to the Researchers Supporting Project number (RSPD2023R765), King Saud University, Riyadh, Saudi Arabia for the financial support.

Appendix A. Supporting information

Supplementary data associated with this article can be found in the online version at doi:10.1016/j.jece.2023.111308.

References

[1] Y. Cong, J. Zhang, F. Chen, M. Anpo, Synthesis and characterization of nitrogen-doped TiO_2 nanophotocatalyst with high visible light activity, J. Phys. Chem. C 111 (2007) 6976–6982.
[2] M.R. Al-Mamun, S. Kader, M.S. Islam, M.Z.H. Khan, Photocatalytic activity improvement and application of UV-TiO_2 photocatalysis in textile wastewater treatment: a review, J. Environ. Chem. Eng. 7 (2019), 103248.
[3] N.T.-T. Hoang, A.T.-K. Tran, T.-A. Le, D.D. Nguyen, Enhancing efficiency and photocatalytic activity of TiO_2-SiO_2 by combination of glycerol for MO degradation in continuous reactor under solar irradiation, J. Environ. Chem. Eng. 9 (2021), 105789.
[4] J.A. Khan, C. Han, N.S. Shah, H.M. Khan, M.N. Nadagouda, V. Likodimos, P. Falaras, K. O'Shea, D.D. Dionysiou, Ultraviolet-visible light-sensitive high surface area phosphorous-fluorine-co-doped TiO_2 nanoparticles for the degradation of atrazine in water, Environ. Eng. Sci. 31 (2014) 435–446.
[5] P.S. Basavarajappa, S.B. Patil, N. Ganganagappa, K.R. Reddy, A.V. Raghu, C. V. Reddy, Recent progress in metal-doped TiO_2, non-metal doped/codoped TiO_2 and TiO_2 nanostructured hybrids for enhanced photocatalysis, Int. J. Hydrog. Energy 45 (2020) 7764–7778.
[6] J.L. Gole, J.D. Stout, C. Burda, Y. Lou, X. Chen, Highly efficient formation of visible light tunable $TiO_{2-x}N_x$ photocatalysts and their transformation at the nanoscale, J. Phys. Chem. B 108 (2004) 1230–1240.
[7] A. Di Paola, G. Marcì, L. Palmisano, M. Schiavello, K. Uosaki, S. Ikeda, B. Ohtani, Preparation of polycrystalline TiO_2 photocatalysts impregnated with various transition metal ions: Characterization and photocatalytic activity for the degradation of 4-nitrophenol, J. Phys. Chem. B 106 (2002) 637–645.
[8] J. Zhu, Z. Deng, F. Chen, J. Zhang, H. Chen, M. Anpo, J. Huang, L. Zhang, Hydrothermal doping method for preparation of Cr^{3+}-TiO_2 photocatalysts with concentration gradient distribution of Cr^{3+}, Appl. Catal. B: Environ. 62 (2006) 329–335.
[9] R. Chauhan, A. Kumar, R.P. Chaudhary, Structural and photocatalytic studies of Mn doped TiO_2 nanoparticles, Spectrochim. Acta, Part A 98 (2012) 256–264.
[10] S. Pang, J.G. Huang, Y. Su, B. Geng, S.Y. Lei, Y.T. Huang, C. Lyu, X.J. Liu, Synthesis and modification of Zn-doped TiO_2 nanoparticles for the photocatalytic degradation of tetracycline, Photochem. Photobiol. 92 (2016) 651–657.
[11] C.-Y. Su, L.-C. Wang, W.-S. Liu, C.-C. Wang, T.-P. Perng, Photocatalysis and hydrogen evolution of Al- and Zn-doped TiO_2 nanotubes fabricated by atomic layer deposition, ACS Appl. Mater. Interfaces 10 (2018) 33287–33295.
[12] H. Sudrajat, S. Babel, A.T. Ta, T.K. Nguyen, Mn-doped TiO_2 photocatalysts: role, chemical identity, and local structure of dopant, J. Phys. Chem. Solids 144 (2020), 109517.
[13] G. Wu, T. Nishikawa, B. Ohtani, A. Chen, Synthesis and characterization of carbon-doped TiO_2 nanostructures with enhanced visible light response, Chem. Mater. 19 (2007) 4530–4537.
[14] C. Han, M. Pelaez, V. Likodimos, A.G. Kontos, P. Falaras, K. O'Shea, D. D. Dionysiou, Innovative visible light-activated sulfur doped TiO_2 films for water treatment, Appl. Catal. B: Environ. 107 (2011) 77–87.
[15] C. Han, J. Andersen, V. Likodimos, P. Falaras, J. Linkugel, D.D. Dionysiou, The effect of solvent in the sol-gel synthesis of visible light-activated, sulfur-doped TiO_2 nanostructured porous films for water treatment, Catal. Today 224 (2014) 132–139.
[16] S.A. Ansari, M.M. Khan, M.O. Ansari, M.H. Cho, Nitrogen-doped titanium dioxide (N-doped TiO_2) for visible light photocatalysis, New J. Chem. 40 (2016) 3000–3009.
[17] J. Xu, Y. Ao, D. Fu, C. Yuan, Low-temperature preparation of F-doped TiO_2 film and its photocatalytic activity under solar light, Appl. Surf. Sci. 254 (2008) 3033–3038.
[18] J. Xu, Y. Ao, D. Fu, C. Yuan, A simple route to synthesize highly crystalline N-doped TiO_2 particles under low temperature, J. Cryst. Growth 310 (19) (2008) 4319–4324.
[19] M. Ismael, A review and recent advances in solar-to-hydrogen energy conversion based on photocatalytic water splitting over doped-TiO_2 nanoparticles, Sol. Energy 211 (2020) 522–546.
[20] J. Chen, F. Qiu, W. Xu, S. Cao, H. Zhu, Recent progress in enhancing photocatalytic efficiency of TiO_2-based materials, Appl. Catal. A: Gen. 495 (2015) 131–140.
[21] P.V. Bakre, S.G. Tilve, R.N. Shirsat, Influence of N sources on the photocatalytic activity of N-doped TiO_2, Arab. J. Chem. 13 (2020) 7637–7651.
[22] S.K. Kassahun, Z. Kiflie, H. Kim, B.T. Gadisa, Effects of operational parameters on bacterial inactivation in Vis-LEDs illuminated N-doped TiO_2 based photoreactor, J. Environ. Chem. Eng. 8 (2020), 104374.
[23] J. Huang, L. Dou, J. Li, J. Zhong, M. Li, T. Wang, Excellent visible light responsive photocatalytic behavior of N-doped TiO_2 toward decontamination of organic pollutants, J. Hazard. Mater. 403 (2021), 123857.
[24] C. Di Valentin, E. Finazzi, G. Pacchioni, A. Selloni, S. Livraghi, M.C. Paganini, E. Giamello, N-doped TiO_2: Theory and experiment, Chem. Phys. 339 (2007) 44–56.
[25] N. Kovalevskiy, D. Selishchev, D. Svintsitskiy, S. Selishcheva, A. Berezin, D. Kozlov, Synergistic effect of polychromatic radiation on visible light activity of N-doped TiO_2 photocatalyst, Catal. Commun. 134 (2020), 105841.
[26] C. Di Valentin, G. Pacchioni, A. Selloni, S. Livraghi, E. Giamello, Characterization of paramagnetic species in N-doped TiO_2 powders by EPR spectroscopy and DFT calculations, J. Phys. Chem. B 109 (2005) 11414–11419.
[27] W.C. Huang, J.-M. Ting, Novel nitrogen-doped anatase TiO_2 mesoporous bead photocatalysts for enhanced visible light response, Ceram. Int. 43 (2017) 9992–9997.
[28] M.-S. Wong, H. Pang Chou, T.-S. Yang, Reactively sputtered N-doped titanium oxide films as visible-light photocatalyst, Thin Solid Films 494 (2006) 244–249.
[29] T.S. Natarajan, V. Mozhiarasi, R.J. Tayade, Nitrogen doped titanium dioxide (N-TiO_2): synopsis of synthesis methodologies, doping mechanisms, property evaluation and visible light photocatalytic applications, Photochem 1 (2021) 371–410.
[30] F. Zhou, H. Song, H. Wang, S. Komarneni, C. Yan, N-doped TiO_2/sepiolite nanocomposites with enhanced visible-light catalysis: Role of N precursors, Appl. Clay Sci. 166 (2018) 9–17.
[31] T. Ma, M. Akiyama, E. Abe, I. Imai, High-efficiency dye-sensitized solar cell based on a nitrogen-doped nanostructured titania electrode, Nano Lett. 5 (2005) 2543–2547.
[32] H. Fakhouri, Thin film deposition of pure and doped TiO_2 by RF magnetron sputtering for visible light photocatalytic and optoelectronic applications, HAL: Archives Ouvertes, Paris, 2012. ⟨https://tel.archives-ouvertes.fr/tel-00825830⟩.
[33] G. Li, B. Zou, S. Feng, H. Shi, K. Liao, Y. Wang, W. Wang, G. Zhang, Synthesis of N-doped TiO_2 with good photocatalytic property, Phys. B: Condens. Matter 588 (2020), 412184.

[34] Y.V. Divyasri, N. Lakshmana Reddy, K. Lee, M. Sakar, V. Navakoteswara Rao, V. Venkatramu, M.V. Shankar, N.C. Gangi Reddy, Optimization of N doping in TiO_2 nanotubes for the enhanced solar light mediated photocatalytic H_2 production and dye degradation, Environ. Pollut. 269 (2021), 116170.

[35] M. Sathish, B. Viswanathan, R.P. Viswanath, C.S.Gopinath Synthesis, characterization, electronic structure, and photocatalytic activity of nitrogen-doped TiO_2 nanocatalyst, Chem. Mater. 17 (2005) 6349–6353.

[36] J. Wang, D.N. Tafen, J.P. Lewis, Z. Hong, A. Manivannan, M. Zhi, M. Li, N. Wu, Origin of photocatalytic activity of nitrogen-doped TiO_2 nanobelts, J. Am. Chem. Soc. 131 (2009) 12290–12297.

[37] P.S. Jadhav, T. Jadhav, M. Bhosale, C.H. Jadhav, V.C. Pawar, Structural and optical properties of N-doped TiO_2 nanomaterials, Mater. Today.: Proc. 43 (2021) 2763–2767.

[38] J. Zhang, D. Liu, W. Bian, X. Chen, Degradation of 2,4-dichorophenol by pulsed high voltage discharge in water, Desalination 304 (2012) 49–56.

[39] K.V. Baiju, C.P. Sibu, K. Rajesh, P.K. Pillai, P. Mukundan, K.G.K. Warrier, W. Wunderlich, An aqueous sol-gel route to synthesize nanosized lanthana-doped titania having an increased anatase phase stability for photocatalytic application, Mater. Chem. Phys. 90 (2005) 123–127.

[40] J.A. Khan, N.S. Shah, H.M. Khan, Decomposition of atrazine by ionizing radiation: Kinetics, degradation pathways and influence of radical scavengers, Sep. Purif. Technol. 156 (2015) 140–147.

[41] S. Sun, P. Gao, Y. Yang, P. Yang, Y. Chen, Y. Wang, N-doped TiO_2 nanobelts with coexposed (001) and (101) facets and their highly efficient visible-light-driven photocatalytic hydrogen production, ACS Appl. Mater. Interfaces 8 (2016) 18126–18131.

[42] Y.-J. Yuan, Z.-J. Ye, H.-W. Lu, B. Hu, Y.-H. Li, D.-Q. Chen, J.-S. Zhong, Z.-T. Yu, Z.-G. Zou, Constructing anatase TiO_2 nanosheets with exposed (001) facets/layered MoS_2 two-dimensional nanojunctions for enhanced solar hydrogen generation, ACS Catal. (2016) 532–541.

[43] J.A. Khan, M. Sayed, N.S. Shah, S. Khan, Y. Zhang, G. Boczkaj, H.M. Khan, D. D. Dionysiou, Synthesis of eosin modified TiO_2 film with co-exposed {001} and {101} facets for photocatalytic degradation of para-aminobenzoic acid and solar H_2 production, Appl. Catal. B: Environ. 265 (2020), 118557.

[44] A. Karci, I. Arslan-Alaton, T. Olmez-Hanci, M. Bekbölet, Transformation of 2,4-dichlorophenol by H_2O_2/UV-C, Fenton and photo-Fenton processes: Oxidation products and toxicity evolution, J. Photochem. Photobiol. A: Chem. 230 (2012) 65–73.

[45] ECOSAR, Ecological Structure Activity Relationships (ECOSAR) Predictive Model, US EPA,, 2014.

[46] F. Ali, J.A. Khan, N.S. Shah, M. Sayed, H.M. Khan, Carbamazepine degradation by UV and UV-assisted AOPs: Kinetics, mechanism and toxicity investigations, Process Saf. Environ. Prot. 117 (2018) 307–314.

[47] A.E.J. González, S.G. Santiago, Structural and optoelectronic characterization of TiO_2 films prepared using the sol-gel technique, Semicond. Sci. Technol. 22 (2007) 709–716.

[48] A.I. Kontos, A.G. Kontos, Y.S. Raptis, P. Falaras, Nitrogen modified nanostructured titania: electronic, structural and visible-light photocatalytic properties, Phys. Stat. Sol. (RRL) 2 (2008) 83–85.

[49] M. Pelaez, A.A. de la Cruz, E. Stathatos, P. Falaras, D.D. Dionysiou, Visible light-activated N-F-codoped TiO_2 nanoparticles for the photocatalytic degradation of microcystin-LR in water, Catal. Today 144 (2009) 19–25.

[50] X. Cheng, X. Yu, Z. Xing, Characterization and mechanism analysis of N doped TiO_2 with visible light response and its enhanced visible activity, Appl. Surf. Sci. 258 (2012) 3244–3248.

[51] G. Sauthier, E. György, A. Figueras, R.S. Sánchez, J. Hernando, Laser synthesis and characterization of nitrogen-doped TiO_2 vertically aligned columnar array photocatalysts, J. Phys. Chem. C. 116 (2012) 14534–14540.

[52] V.J. Babu, M.K. Kumar, A.S. Nair, T.L. Kheng, S.I. Allakhverdiev, S. Ramakrishna, Visible light photocatalytic water splitting for hydrogen production from N-TiO_2 rice grain shaped electrospun nanostructures, Int. J. Hydrog. Energy 37 (2012) 8897–8904.

[53] K.S.W. Sing, Reporting physisorption data for gas/solid systems with special reference to the determination of surface area and porosity (Recommendations 1984), Pure Appl. Chem. 57 (1985) 603–619.

[54] B. Prasai, B. Cai, M.K. Underwood, J.P. Lewis, D.A. Drabold, Properties of amorphous and crystalline titanium dioxide from first principles, J. Mater. Sci. 47 (2012) 7515–7521.

[55] Y. Zhang, J. Wan, Y. Ke, A novel approach of preparing TiO_2 films at low temperature and its application in photocatalytic degradation of methyl orange, J. Hazard. Mater. 177 (2010) 750–754.

[56] A. Sanchez-Martinez, O. Ceballos-Sanchez, C. Koop-Santa, E.R. López-Mena, E. Orozco-Guareño, M. García-Guaderrama, N-doped TiO_2 nanoparticles obtained by a facile coprecipitation method at low temperature, Ceram. Int. 44 (2018) 5273–5283.

[57] L. Zeng, W. Song, M. Li, X. Jie, D. Zeng, C. Xie, Comparative study on the visible light driven photocatalytic activity between substitutional nitrogen doped and interstitial nitrogen doped TiO_2, Appl. Catal. A: Gen. 488 (2014) 239–247.

[58] M. Sayed, B. Ren, A.M. Ali, A. Al-Anazi, M.N. Nadagouda, A.A. Ismail, D. D. Dionysiou, Solar light induced photocatalytic activation of peroxymonosulfate by ultra-thin Ti^{3+} self-doped Fe_2O_3/TiO_2 nanoflakes for the degradation of naphthalene, Appl. Catal. B: Environ. 315 (2022), 121532.

[59] B. Palanisamy, C.M. Babu, B. Sundaravel, S. Anandan, V. Murugesan, Sol-gel synthesis of mesoporous mixed Fe_2O_3/TiO_2 photocatalyst: Application for degradation of 4-chlorophenol, J. Hazard. Mater. 252–253 (2013) 233–242.

[60] H. Khan, I.K. Swati, Fe^{3+}-doped anatase TiO_2 with d–d transition, oxygen vacancies and Ti^{3+} centers: synthesis, characterization, UV–vis photocatalytic and mechanistic studies, Ind. Eng. Chem. Res. 55 (2016) 6619–6633.

[61] X. Jiang, Y. Zhang, J. Jiang, Y. Rong, Y. Wang, Y. Wu, C. Pan, Characterization of oxygen vacancy associates within hydrogenated TiO_2: a positron annihilation study, J. Phys. Chem. C. 116 (2012) 22619–22624.

[62] H. Liu, H. Fan, R. Wu, L. Tian, X. Yang, Y. Sun, Nitrogen-doped black TiO_2 spheres with enhanced visible light photocatalytic performance, SN Appl. Sci. 1 (2019) 487.

[63] B. Zhao, X. Wang, Y. Zhang, J. Gao, Z. Chen, Z. Lu, Synergism of oxygen vacancies, Ti^{3+} and N dopants on the visible-light photocatalytic activity of N-doped TiO_2, J. Photochem. Photobiol. A: Chem. 382 (2019), 111928.

[64] A. Wafi, E. Szabó-Bárdos, O. Horváth, É. Makó, M. Jakab, B. Zsirka, Coumarin-based quantification of hydroxyl radicals and other reactive species generated on excited nitrogen-doped TiO_2, J. Photochem. Photobiol. A: Chem. 404 (2021), 112913.

[65] M. Naushad, G. Sharma, Z.A. Alothman, Photodegradation of toxic dye using Gum Arabic-crosslinked-poly(acrylamide)/$Ni(OH)_2$/FeOOH nanocomposites hydrogel, J. Clean. Prod. 241 (2019), 118263.

[66] C. Zhao, M. Pelaez, X. Duan, H. Deng, K. O'Shea, D. Fatta-Kassinos, D.D. Dionysiou, Role of pH on photolytic and photocatalytic degradation of antibiotic oxytetracycline in aqueous solution under visible/solar light: Kinetics and mechanism studies, Appl. Catal. B: Environ. 134–135 (2013) 83–92.

[67] J. Peller, P.V. Kamat, Radiolytic transformations of chlorinated phenols and chlorinated phenoxyacetic acids, J. Phys. Chem. A 109 (2005) 9528–9535.

[68] A.L. Garcia-Costa, A. Alves, L.M. Madeira, M.S.F. Santos, Oxidation processes for cytostatic drugs elimination in aqueous phase: a critical review, J. Environ. Chem. Eng. 9 (2021), 104709.

[69] J.A. Khan, X. He, N.S. Shah, H.M. Khan, E. Hapeshi, D. Fatta-Kassinos, D. D. Dionysiou, Kinetic and mechanism investigation on the photochemical degradation of atrazine with activated H_2O_2, $S_2O_8^{2-}$ and HSO_5^-, Chem. Eng. J. 252 (2014) 393–403.

[70] J.A. Khan, X. He, H.M. Khan, N.S. Shah, D.D. Dionysiou, Oxidative degradation of atrazine in aqueous solution by UV/H_2O_2/Fe^{2+}, UV/$S_2O_8^{2-}$/Fe^{2+} and UV/HSO_5^-/Fe^{2+} processes: A comparative study, Chem. Eng. J. 218 (2013) 376–383.

[71] E. Brillas, S. Garcia-Segura, Recent progress of applied TiO_2 photoelectrocatalysis for the degradation of organic pollutants in wastewaters, J. Environ. Chem. Eng. 11 (2023), 109635.

[72] J.A. Khan, X. He, N.S. Shah, M. Sayed, H.M. Khan, D.D. Dionysiou, Degradation kinetics and mechanism of desethyl-atrazine and desisopropyl-atrazine in water with $^{\bullet}OH$ and $SO_4^{\bullet-}$ based-AOPs, Chem. Eng. J. 325 (2017) 485–494.

[73] T. An, J. An, Y. Gao, G. Li, H. Fang, W. Song, Photocatalytic degradation and mineralization mechanism and toxicity assessment of antivirus drug acyclovir: Experimental and theoretical studies, Appl. Catal. B: Environ. 164 (2015) 279–287.

[74] N. Zhong, M. Chen, Y. Luo, Z. Wang, X. Xin, B.E. Rittmann, A novel photocatalytic optical hollow-fiber with high photocatalytic activity for enhancement of 4-chlorophenol degradation, Chem. Eng. J. 355 (2019) 731–739.

[75] J. Di, J. Chen, M. Ji, Q. Zhang, L. Xu, J. Xia, H. Li, Reactable ionic liquid induced homogeneous carbon superdoping of $BiPO_4$ for superior photocatalytic removal of 4-chlorophenol, Chem. Eng. J. 313 (2017) 1477–1485.

[76] P. Chang, Y. Wang, Y. Wang, Y. Zhu, Current trends on In_2O_3 based heterojunction photocatalytic systems in photocatalytic application, Chem. Eng. J. 450 (2022), 137804.

[77] Q. Shi, H. Wang, S. Liu, Z. Bian, Electrocatalytic degradation of 2,4-dichlorophenol using a Pd/graphene gas-diffusion electrode, RSC Adv. 4 (2014) 56263–56272.

[78] H. Wang, Y. Zhao, Y. Su, T. Li, M. Yao, C. Qin, Fenton-like degradation of 2,4-dichlorophenol using calcium peroxide particles: performance and mechanisms, RSC Adv. 7 (2017) 4563–4571.

[79] Q. Lian, A. Roy, O. Kizilkaya, D.D. Gang, W. Holmes, M.E. Zappi, X. Zhang, H. Yao, Uniform mesoporous amorphous cobalt-inherent silicon oxide as a highly active heterogeneous catalyst in the activation of peroxymonosulfate for rapid oxidation of 2,4-dichlorophenol: The important role of inherent cobalt in the catalytic mechanism, ACS Appl. Mater. Interfaces 12 (2020) 57190–57206.

[80] T. Luo, Z. Ai, L. Zhang, Fe@Fe_2O_3 core-shell nanowires as iron reagent. 4. Sono-Fenton degradation of pentachlorophenol and the mechanism analysis, J. Phys. Chem. C. 112 (2008) 8675–8681.

[81] X. Chen, Y. Dai, J. Guo, T. Liu, X. Wang, Novel magnetically separable reduced graphene oxide (RGO)/$ZnFe_2O_4$/Ag_3PO_4 nanocomposites for enhanced photocatalytic performance toward 2,4-dichlorophenol under visible light, Ind. Eng. Chem. Res. 55 (2016) 568–578.

[82] M.K. Kumar, K. Bhavani, B. Srinivas, S.N. Kumar, M. Sudhakar, G. Naresh, A. Venugopal, Nano structured bismuth and nitrogen co-doped TiO_2 as an efficient light harvesting photocatalyst under natural sunlight for the production of H_2 by H_2O splitting, Appl. Catal. A: Gen. 515 (2016) 91–100.

[83] B.-S. Huang, M.-Y. Wey, Properties and H_2 production ability of Pt photodeposited on the anatase phase transition of nitrogen-doped titanium dioxide, Int. J. Hydrog. Energy 36 (2011) 9479–9486.

[84] Q. Xiang, J. Yu, W. Wang, M. Jaroniec, Nitrogen self-doped nanosized TiO_2 sheets with exposed {001} facets for enhanced visible-light photocatalytic activity, Chem. Commun. 47 (2011) 6906–6908.
[85] X. Zhang, P. Song, X. Cui, Nitrogen-doped TiO_2 photocatalysts synthesized from titanium nitride: characterizations and photocatalytic hydrogen evolution performance, J. Adv. Oxid. Technol. 16 (2013) 131–136.
[86] L. Yao, H. Wang, Y. Zhang, S. Wang, X. Liu, Fabrication of N doped TiO_2/C nanocomposites with hierarchical porous structure and high photocatalytic activity, Microporous Mesoporous Mater. 288 (2019), 109604.
[87] H.G. Kim, D.W. Hwang, J. Kim, Y.G. Kim, J.S. Lee, Highly donor-doped (110) layered perovskite materials as novel photocatalysts for overall water splitting, Chem. Commun. (1999) 1077–1078.
[88] Q. Xiang, J. Yu, M. Jaroniec, Synergetic effect of MoS_2 and graphene as cocatalysts for enhanced photocatalytic H_2 production activity of TiO_2 nanoparticles, J. Am. Chem. Soc. 134 (2012) 6575–6578.
[89] M.-C. Wu, J. Hiltunen, A. Sápi, A. Avila, W. Larsson, H.-C. Liao, M. Huuhtanen, G. Tóth, A. Shchukarev, N. Laufer, Á. Kukovecz, Z. Kónya, J.-P. Mikkola, R. Keiski, W.-F. Su, Y.-F. Chen, H. Jantunen, P.M. Ajayan, R. Vajtai, K. Kordás, Nitrogen-doped anatase nanofibers decorated with noble metal nanoparticles for photocatalytic production of hydrogen, ACS Nano 5 (2011) 5025–5030.
[90] J. Kwon, K. Choi, M. Schreck, T. Liu, E. Tervoort, M. Niederberger, Gas-phase nitrogen doping of monolithic TiO_2 nanoparticle-based aerogels for efficient visible light-driven photocatalytic H_2 Production, ACS Appl. Mater. Interfaces 13 (2021) 53691–53701.
[91] G. Liu, T. Zhang, T. Wang, H. Yamashita, Y. Zhao, X. Qian, Peroxydisulfate activation by photo-generated charges on mesoporous carbon nitride for removal of chlorophenols, Appl. Catal. B: Environ. 296 (2021), 120370.
[92] M. Chu, K. Hu, J. Wang, Y. Liu, S. Ali, C. Qin, L. Jing, Synthesis of g-C_3N_4-based photocatalysts with recyclable feature for efficient 2,4-dichlorophenol degradation and mechanisms, Appl. Catal. B: Environ. 243 (2019) 57–65.